15-Lipoxygenase-Mediated Lipid Peroxidation Regulates LRRK2 Kinase Activity

Authors:
Matthew T. Keeney[1,2,3], Eric K. Hoffman[1,2], Julie Weir[1,2], Weston G. Wagner[1,2], Emily M. Rocha[1,2], Sandra Castro[1,2], Kyle Farmer[1,2], Marco Fazzari[3], Roberto Di Maio[1,2] Andrei Konradi[4], Teresa G. Hastings[1,2], Sean A. Pintchovski[4], William D. Shrader[4], J. Timothy Greenamyre[1,2*]

Affiliations:
[1]Pittsburgh Institute for Neurodegenerative Diseases, University of Pittsburgh School of Medicine, Pittsburgh, Pennsylvania.
[2]Department of Neurology, University of Pittsburgh School of Medicine, Pittsburgh, Pennsylvania.
[3]Department of Pharmacology and Chemical Biology, University of Pittsburgh School of Medicine, Pittsburgh, Pennsylvania.
[4]Acurex Biosciences, San Carlos, California.

***Corresponding author:** J. Timothy Greenamyre
University of Pittsburgh
3501 Fifth Avenue, Suite 7039
Pittsburgh, PA 15260

Tel: 412-648-9793
Fax: 412-648-9766
Email: jgreena@pitt.edu

One Sentence Summary: *15-Lipoxygenase-derived 4-HNE stimulates LRRK2 kinase activity*

ABSTRACT: Mutations in *leucine-rich repeat kinase 2 (LRRK2)* that increase its kinase activity are strongly linked to genetic forms of Parkinson's disease (PD). However, the regulation of endogenous wild-type (WT) LRRK2 kinase activity remains poorly understood, despite its frequent elevation in idiopathic PD (iPD) patients. Various stressors such as mitochondrial dysfunction, lysosomal dyshomeostasis, or vesicle trafficking deficits can activate WT LRRK2 kinase, but the specific molecular mechanisms are not fully understood. We found that the production of 4-hydroxynonenal (4-HNE), a lipid hydroperoxidation end-product, is a common biochemical response to these diverse stimuli. 4-HNE forms post-translational adducts with Cys2024 and Cys2025 in the kinase activation loop of WT LRRK2, significantly increasing its kinase activity. Additionally, we discovered that the 4-HNE responsible for regulating LRRK2 is generated by the action of 15-lipoxygenase (15-LO), making 15-LO an upstream regulator of the pathogenic hyperactivation of LRRK2 kinase activity. Pharmacological inhibition or genetic ablation of 15-LO prevents 4-HNE post-translational modification of LRRK2 kinase and its subsequent pathogenic hyperactivation. Therefore, 15-LO inhibitors, or methods to lower 4-HNE levels, or the targeting of Cys2024/2025 could provide new therapeutic strategies to modulate LRRK2 kinase activity and treat PD.

58 **Main Text:**

59 **INTRODUCTION**

60 Missense mutations in *leucine-rich repeat kinase 2* (LRRK2) are a common cause of familial
61 Parkinson's disease (PD) (*1, 2*) . Both coding and non-coding variants in *LRRK2* have been shown
62 to increase the risk of developing PD (*3, 4*). Most of these mutations are located in the Roc-Cor
63 GTPase or kinase domain of LRRK2 and often result in elevated kinase activity, leading to a toxic
64 gain-of-function (*1, 2, 5, 6*). Evidence also suggests wild-type (WT) LRRK2 kinase activity is
65 enhanced in idiopathic PD (iPD) (*7-11*). Thus, LRRK2 might be a link between genetic and
66 idiopathic forms of PD. However, the upstream signaling mechanisms that promote WT LRRK2
67 kinase activation are not well understood.

68

69 LRRK2 uses a classical kinase switch activation mechanism (*12*), where the dynamics of the
70 kinase domain drive its activation (*13*). Upon activation, LRRK2 phosphorylates its substrates,
71 including a subset of Rab GTPases (e.g., Rab10 and Rab12) (*14, 15*), which regulate
72 endolysosomal function (*8*). Excessive LRRK2 kinase activity can also cause endolysosomal
73 dysfunction, creating a complex feedback loop.

74

75 The kinase domain of LRRK2 is similar to the redox-sensitive MAP kinase, ASK1 (*16*), which
76 undergoes redox-induced functional changes. Redox stress, long implicated in PD pathogenesis,
77 can induce WT LRRK2 kinase activity (*5, 9, 17, 18*), potentially to the same extent as the kinase
78 activating G2019S mutation (*9, 18*). Interestingly, LRRK2 can be activated by various stimuli that
79 induce oxidative damage, lysosomal damage, membrane rupture or remodeling, vesicular
80 trafficking deficits, and signaling through Stimulator of Interferon Genes (STING) (*19-24*).

A potential common factor among these stimuli is their association with membrane damage and lipid peroxidation, leading to the accumulation of 4-hydroxynonenal (4-HNE), a reactive aldehyde that plays a role in activating other kinases (*25-28*). The formation of 4-HNE occurs either nonenzymatically when lipids react with reactive oxygen species (ROS), or enzymatically through the hydroperoxidation of membrane phospholipids by lipoxygenase enzymes, primarily 15-lipoxygenase (15-LO) (*29, 30*). 4-HNE can form irreversible Michael-adducts with cysteine residues, and the kinase activation loop of LRRK2 contains highly conserved, solvent-exposed, vicinal cysteine residues, Cys2024 and Cys2025, which may be important for redox sensing (*12*).

Here, we provide evidence that oxidative stimulation of endogenous LRRK2 kinase activity by H_2O_2, rotenone, chloroquine, or monensin depends on cysteine residues, Cys2024 and Cys2025, and involves the formation of adducts between 4-HNE and LRRK2. Importantly, blocking 4-HNE production with a 15-LO inhibitor, or through genetic ablation of 15-LO, prevents pathologically elevated LRRK2 kinase activation without affecting basal LRRK2 kinase activity.

99 **RESULTS**

100 ***Stimulated endogenous LRRK2 activity is redox dependent***

101 The regulation of WT LRRK2 kinase activity remains poorly understood, but evidence suggests it
102 is sensitive to redox stress (*8*). Several reports indicate that LRRK2 kinase activity increases with
103 H_2O_2 and decreases with the antioxidant curcumin (*9, 18, 31, 32*). WT endogenous LRRK2 kinase
104 activity can be elevated dose-dependently by physiological concentrations of H_2O_2, and this can
105 be blocked by α-tocopherol (*9*), which is both an antioxidant and a 15-LO inhibitor (*33*). To further
106 investigate this regulation, we examined the *in situ* kinetics of H_2O_2-induced endogenous WT
107 LRRK2 activation in human embryonic kidney 293 cells (HEK293). Cells treated with 5μM H_2O_2
108 for 5, 10, and 15 minutes showed a robust increase in LRRK2 kinase activity, as detected by
109 proximity ligation (PL) assay for the phosphorylation status of the autophosphorylation site
110 Ser1292 (PL pS1292–LRRK2) (*9, 34*). This signal was maximal at 10 minutes and sustained for
111 at least 30 minutes (***Fig. 1A, B***). Pretreatment of cells with a thiol antioxidant, N-acetylcysteine
112 (NAC), prevented the H_2O_2-induced increase in PL pS1292-LRRK2 signal ($p<0.0001$; two-way
113 analysis of variance (ANOVA) with Tukey correction) (***Fig, 1C, D***), confirming the redox
114 sensitivity of LRRK2 kinase activation.

115

116
117

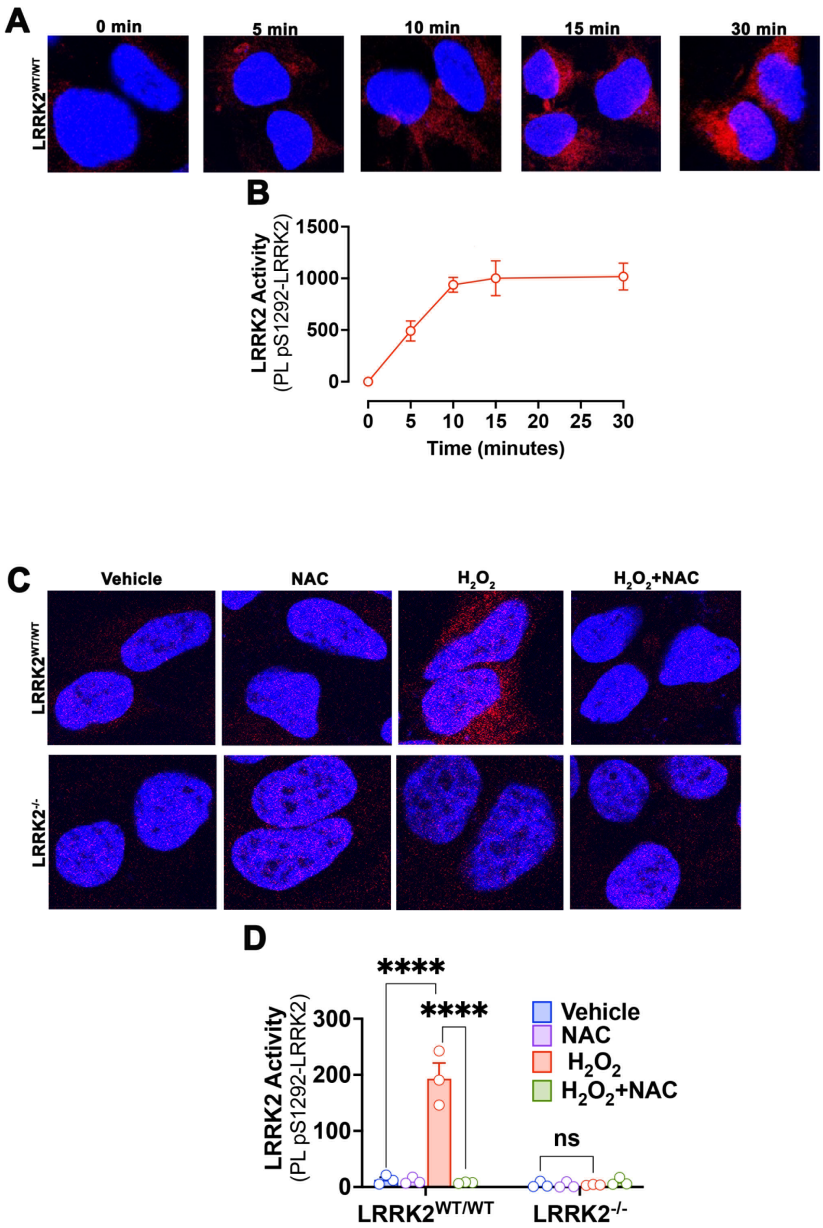

Figure 1. H_2O_2 elicits rapid LRRK2 autophosphorylation. (**A**) Endogenous LRRK2 kinase activity was assessed by proximity ligation (PL) assay between pS1292 and total LRRK2 (PL pS1292–LRRK2) in $LRRK2^{WT/WT}$ HEK293 cells treated with 5μM H_2O_2 for 5, 10, 15, or 30 minutes. A robust increase in PL pS1292-LRRK2 signal (red) was observed within 10 minutes of treatment and remained sustained. (**B**) Quantification of the time course of LRRK2 activity in response to H_2O_2. Each symbol represents the average PL pS1292-LRRK2 fluorescence intensity from 4 independent experiments obtained from 100-150 cells per treatment group for each independent experiment. (**C**) H_2O_2 (5μM) induced LRRK2 kinase activity was assessed by PL pS1292-LRRK2 in $LRRK2^{WT/WT}$ and $LRRK2^{-/-}$ HEK293 cells. H_2O_2 caused a significant increase in PL pS1292-LRRK2 signal in $LRRK2^{WT/WT}$ compared to vehicle. Pretreatment with NAC prevented the H_2O_2-induced increase in PL pS1292-LRRK2 signal, and no signal was detected in $LRRK2^{-/-}$ cells. (**D**) Quantification of LRRK2 activity by PL fluorescence signal. Each symbol represents the average PL pS1292–LRRK2 fluorescence intensity obtained from 100-150 cells per treatment group in three independent experiments. Statistical testing by two-way ANOVA with Tukey correction; ****denotes $p<0.0001$; ns denotes not significant.

134 Activation of WT LRRK2 occurs in response to various cellular stressors, including mitochondrial
135 dysfunction, lysosomal dyshomeostasis, and vesicular trafficking deficits (*9, 20-22, 35*). We
136 explored whether known LRRK2 activators such as rotenone, chloroquine, and monensin activate
137 LRRK2 via a redox mechanism. Rotenone, a mitochondrial complex I inhibitor, increases ROS
138 production, redox stress, and mitochondrial dysfunction in cells (*36*). In WT HEK293 cells,
139 sublethal rotenone treatment elicited an increase in PL pS1292-LRRK2 signal compared to vehicle
140 ($p<0.0001$; two-way ANOVA with Tukey correction) (***Fig. 2A, B***), and this increase was prevented
141 by co-treatment with NAC ($p<0.0001$; two-way ANOVA with Tukey correction) (***Fig. 2A, B***).
142 Congruent results were obtained by western blotting for the phosphorylation state of the LRRK2
143 substrate, Rab10 (*14*) (***fig. S1A, B)***. Rotenone treatment increased pT73-Rab10 levels compared
144 to vehicle ($p<0.05$; two-way ANOVA with Tukey correction), and this increase was prevented by
145 NAC co-treatment ($p<0.05$; one-way ANOVA with Tukey correction) (***fig. S1A, B***). We confirmed
146 these findings using a third method, a PL assay to amplify the specific signal of pT73-Rab10: PL
147 pT73(Rab10)-Rab10 ***(fig. S2)***. Using this assay, there was a baseline pT73(Rab10)-Rab10 signal
148 in WT HEK293 cells that was reduced in the presence of the LRRK2 kinase inhibitor, PF360
149 ($p<0.0001$; two-way ANOVA with Tukey correction) (***fig S2A, B***). Importantly, the baseline
150 pT73(Rab10)-Rab10 signal in WT HEK293 cells was higher than that in LRRK2$^{-/-}$ HEK293 cells
151 ($p<0.0001$; two-way ANOVA with Tukey correction) (***fig S2A, B).*** Similar to the results obtained
152 with PL pS1292-LRRK2 and pT73-Rab10 western blotting, rotenone elicited an increase in PL
153 pT73(Rab10)-Rab10 signal ($p<0.0005$; two-way ANOVA with Tukey correction), that was
154 prevented by co-treatment with NAC ($p<0.0001$; two-way ANOVA with Tukey correction) (***fig.***
155 ***S1D, E***).
156

157 Given the high expression of LRRK2 in immune cells and its role in inflammatory responses in
158 PD, we assessed whether rotenone-induced kinase activation was also redox-dependent in
159 RAW264.7 macrophages. Consistent with the results in HEK293 cells, rotenone increased
160 endogenous LRRK2 activity as measured by PL pS1292-LRRK2 in WT RAW264.7 macrophages
161 (***Fig. 2A, C).*** Co-treatment with NAC prevented the rotenone-induced increase in PL pS1292–
162 LRRK2 signal ($p<0.005$; two-way ANOVA with Tukey correction) (***Fig. 2A, C)***. Similar results
163 were obtained using the orthogonal assays of pT73-Rab10 detection by western blot ($p<0.05$; two-
164 way ANOVA with Tukey correction) (***fig. S1A, C)*** and PL pT73(Rab10)-Rab10 ($p<0.0001$; two-
165 way ANOVA with Tukey correction) (***fig. S1D, F***). Treatment with NAC effectively blocked the
166 rotenone-induced increase in pT73-Rab10 western blot signal ($p<0.05$; two-way ANOVA with
167 Tukey correction) (***fig. S1A, C)*** and PL pT73(Rab10)-Rab10 signal ($p<0.0001$; two-way ANOVA
168 with Tukey correction) (***fig. S1D, F***). Thus, using three separate assays (PL pS1292-LRRK2,
169 pT73-Rab10 western blot, and PL pT73(Rab10)-Rab10) and two different cell lines (HEK293 and
170 RAW264.7 macrophages), we found that rotenone stimulates endogenous LRRK2 kinase activity
171 in a redox-dependent manner.
172
173 As noted, disruption of endolysosomal function or trafficking using chloroquine or monensin
174 activates WT LRRK2 kinase (*21, 22, 35*). However, the mechanisms by which these disturbances
175 in the endolysosomal system regulate LRRK2 kinase activity remain unclear. Given our findings
176 with rotenone, we examined whether chloroquine or monensin activates LRRK2 kinase in a redox-
177 dependent fashion. First, we assessed if chloroquine or monensin causes ROS production or
178 oxidative damage. Using parameters known to elicit endogenous LRRK2 activity (chloroquine:
179 100 μM for 3 hours (*35*); monensin: 10 μM for 4 hours (*22*)) we measured cytoplasmic superoxide
180 production using dihydroethidium (DHE). Under these conditions, both chloroquine and monensin

181 elicited a significant increase in DHE signal compared to vehicle ($p<0.005$; one-way ANOVA with
182 Tukey correction) (***fig. S3A, B***) in WT HEK293 cells. Thus, these stressors cause ROS production
183 at concentrations and time points associated with elevated LRRK2 kinase activity.
184
185 As an orthogonal approach to assess if chloroquine and monensin lead to oxidative damage, we
186 examined if they lead to the accumulation of the omega-6 PUFA-derived lipid hydroperoxidation
187 end-product, 4-HNE. Consistent with the ROS production it induced, chloroquine caused an
188 increase in 4-HNE at 1 hour ($p<0.05$; two-way ANOVA with Tukey correction) and 3 hours
189 ($p<0.001$; two-way ANOVA with Tukey correction), which was prevented by co-treatment with
190 NAC (***fig. S3E, F)***. Similarly, monensin caused an increase in 4-HNE at 4 hours ($p<0.001$; two-
191 way ANOVA with Tukey correction), which was prevented by co-treatment with NAC (***fig. S3G,***
192 ***H)***. Given that these LRRK2 kinase activators cause ROS production and lipid peroxidation, both
193 of which are prevented by NAC, we investigated whether NAC could prevent chloroquine- or
194 monensin-induced LRRK2 kinase activity. Indeed, both chloroquine (***Fig. 2D, E***) and monensin
195 (***Fig. 2F, G)*** treatment of WT HEK293 cells led to an increase in PL pS1292–LRRK2 signal
196 ($p<0.0001$; two-way ANOVA with Tukey correction) that was prevented by NAC co-treatment.
197 Together, these results indicate that known LRRK2 kinase activators, which result in either
198 mitochondrial dysfunction (rotenone), lysosomal dyshomeostasis (chloroquine), or vesicular
199 trafficking deficits (monensin), may activate LRRK2 through a common redox mechanism.
200

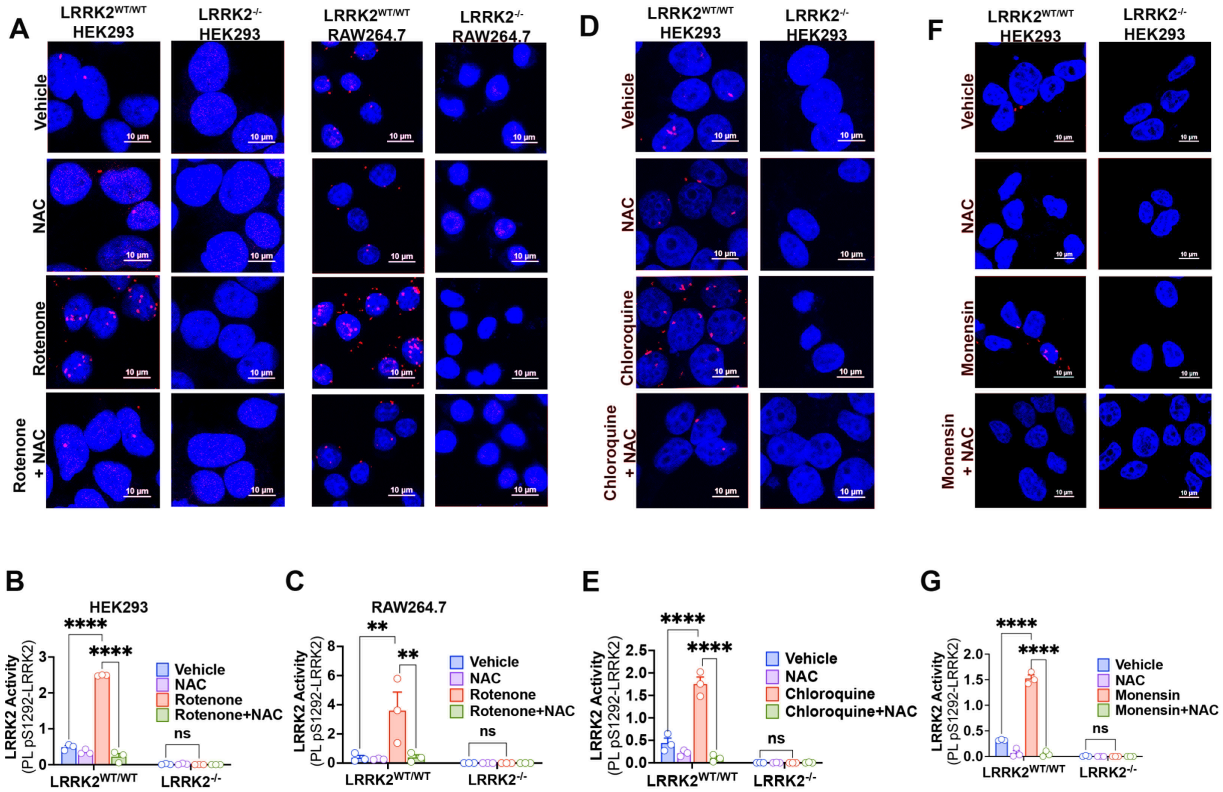

Figure 2. Stimulated LRRK2 activity is ROS dependent. (**A**) Rotenone (50nM) induced LRRK2 kinase activity was assessed by PL pS1292-LRRK2 in LRRK2$^{WT/WT}$ and LRRK2$^{-/-}$ HEK293 cells and RAW264.7 macrophages. Rotenone treatment led to an increase in PL pS1292-LRRK2 (red dots) in both LRRK2$^{WT/WT}$ HEK293 and RAW264.7 macrophages compared to the vehicle. NAC co-treatment prevented rotenone-induced PL pS1292-LRRK2 signal and no signal was detected in LRRK2$^{-/-}$ cells. (**B**) Quantification of LRRK2 activity by PL pS1292–LRRK2 Objects/DAPI in HEK293 cells. (**C**) Quantification of PL pS1292–LRRK2 Objects/DAPI in RAW264.7 macrophages. (**D**) Chloroquine (100µM) and (**F**) Monensin (10µM) elicited an increase in PL pS1292-LRRK2 signal in LRRK2$^{WT/WT}$ HEK293 cells. NAC co-treatment prevented both (**D**) chloroquine and (**F**) monensin-induced PL pS1292-LRRK2 signal. No signal was observed in LRRK2$^{-/-}$ cells. Quantification of LRRK2 activity by PL pS1292–LRRK2 in the presence of (**E**) chloroquine or (**G**) monensin. For each graph **(B, C, E, G)**, each symbol represents the average number of PL pS1292-LRRK2 objects/DAPI obtained from 100-150 cells per treatment group for each of three independent experiments. Statistical testing by two-way ANOVA with post-hoc Tukey correction. **denotes $p<0.005$; ****denotes $p<0.0001$; ns denotes not significant.

220 ***Kinase activation loop cysteines 2024 and 2025 are important for redox-dependent***
221 ***activation of LRRK2***

222 The dynamics of the kinase activation loop plays a critical role in driving LRRK2 kinase activity
223 (*12, 13*). The activation loop contains two cysteine residues, Cys2024 and Cys2025 (*37*), that are
224 highly conserved across many species (*38*) but not present in LRRK1 (*39*), suggesting a specific
225 role in LRRK2 function. Cysteine residues on proteins can undergo modifications affecting
226 function (*25-28*). We hypothesized that Cys2024 and Cys2025 are important for sensing the redox
227 state of the local subcellular environment (*12*) and thereby for regulating LRRK2 kinase activation.
228 Using CRISPR/Cas9, we generated HEK293 cell lines with each of these cysteines mutated
229 individually to an alanine ($LRRK2^{C2024A}$ and $LRRK2^{C2025A}$) or together in a double mutant
230 ($LRRK2^{C2024A+C2025A}$). To ensure that we did not create "kinase-dead" mutants, baseline LRRK2
231 kinase activity was assessed using two assays: PL pS1292–LRRK2 and PL pT73(Rab10)-Rab10
232 (***fig S4A-D***). Under basal conditions, $LRRK2^{C2024A}$, $LRRK2^{C2025A}$, and $LRRK2^{C2024A+C2025A}$ cells
233 had PL pS1292-LRRK2 and PL pT73(Rab10)-Rab10 signals equivalent to $LRRK2^{WT/WT}$ (***fig S4A-***
234 ***D***). Importantly, PF360 treatment decreased basal PL pS1292-LRRK2 and PL pT73(Rab10)-
235 Rab10 signals ($p<0.0001$; two-way ANOVA with Tukey correction) (***fig S4A-D***) in all cell lines.
236

237 Having demonstrated that that baseline kinase activity of endogenous LRRK2 was not reduced in
238 any of the cysteine mutant cell lines, we examined their responses to redox challenges. We found
239 that while H_2O_2 exposure elevated PL pS1292–LRRK2 signal in WT HEK293 cells ($p<0.0001$;
240 two-way ANOVA with Tukey correction), there was no increase in PL pS1292–LRRK2 signal in
241 any of the cysteine mutant cell lines (***Fig. 3A, B)***. Next we explored if rotenone, chloroquine, or
242 monensin were able to enhance kinase activity in $LRRK2^{C2024A}$, $LRRK2^{C2025A}$, and

243 LRRK2$^{C20284A+C2025A}$ HEK293 cells. In WT HEK293 cells, rotenone, chloroquine, and monensin
244 treatment each led to an increase in PL pS1292–LRRK2 signal compared to vehicle ($p<0.0001$;
245 two-way ANOVA with Tukey correction) (***Fig. 3C-H*****).** Strikingly, in LRRK2^{C2024A}, LRRK2^{C2025A},
246 and LRRK2$^{C2024A+C2025A}$ cells there was no increase in PL pS1292–LRRK2 signal in response to
247 rotenone, chloroquine, or monensin (***Fig. 3C-H***).
248
249 It was previously shown that endogenous LRRK2 activity regulates rotenone-induced ROS
250 production (*40, 41*). To assess whether mutating these cysteine residues (thereby blocking the
251 ability of rotenone to stimulate LRRK2 kinase activity) had downstream effects, we measured
252 rotenone-induced ROS production in each of the cell lines (***fig S5***). Rotenone treatment led to an
253 increase in DHE signal in WT HEK293 cells ($p<0.0001$; two-way ANOVA with Tukey correction)
254 but not in LRRK2^{C2024A}, LRRK2^{C2025A} or LRRK2$^{C2024A+C2025A}$ cells (***fig S5***). Together, these results
255 indicate that Cys2024 and Cys2025 are important residues that regulate kinase activation in a
256 redox-responsive fashion.

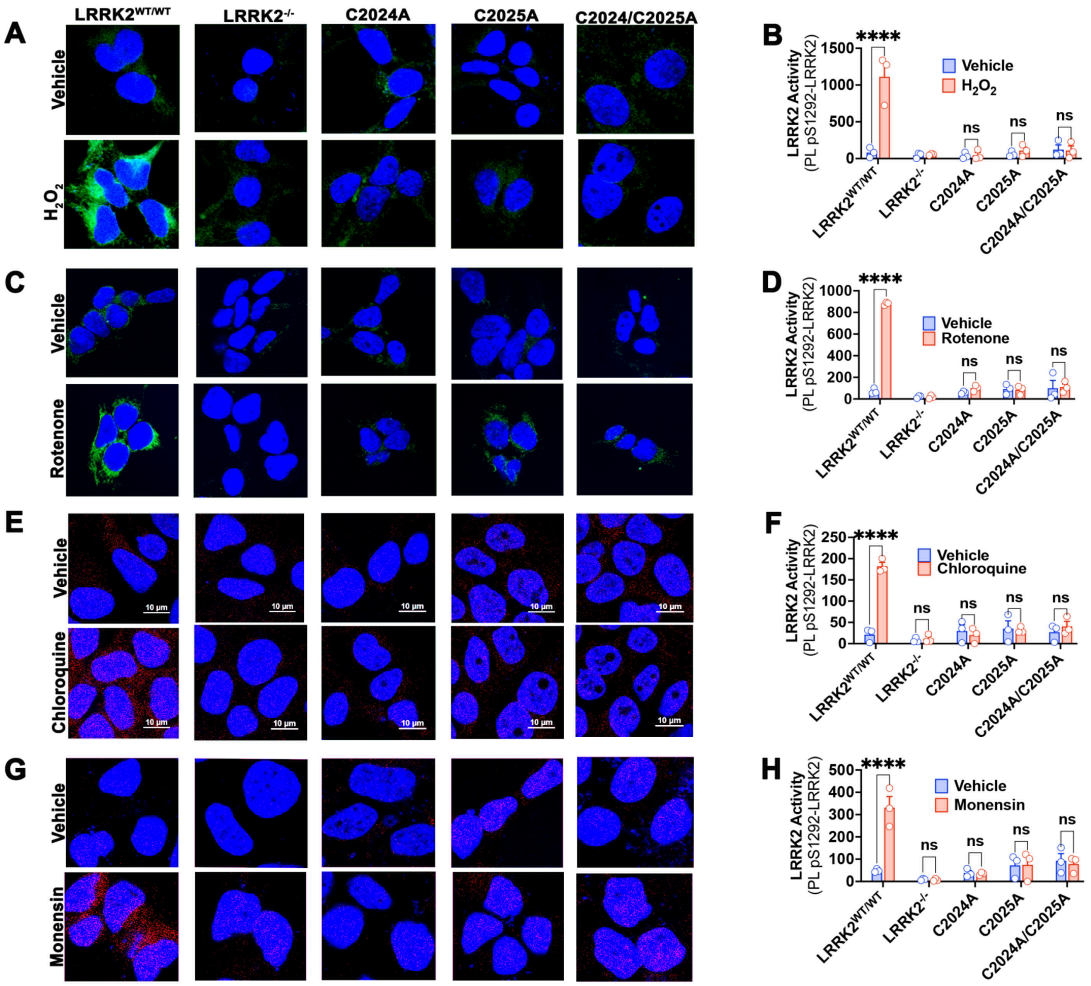

Figure 3. Cys2024 and Cys2025 are important for stimulating LRRK2 kinase activity. Endogenous LRRK2 kinase activity was assessed by PL pS1292-LRRK2 in $LRRK2^{WT/WT}$, $LRRK2^{C2024A}$, $LRRK2^{C2025A}$, and $LRRK2^{C2024A+C2025A}$ (denoted as C2024A, C2025A, C2024A/C2025A respectively) HEK293 cells. (**A**) H_2O_2 (5µM) (**C**) rotenone (50nM) (**E**) chloroquine (100µM) and (**G**) monensin (10µM) elicited an increase in PL pS1292-LRRK2 signal in $LRRK2^{WT/WT}$, which was prevented in $LRRK2^{C2024A}$, $LRRK2^{C2025A}$, and $LRRK2^{C2024A+C2025A}$ HEK293 cells. Note that the PL signal is green for H_2O_2 and rotenone and red for chloroquine and monensin. No signal was observed in $LRRK2^{-/-}$ cells (**A, C, E, G**). Quantification of LRRK2 activity by PL pS1292–LRRK2 fluorescence signal in presence of (**B**) H_2O_2, (**D**) rotenone, (**F**) chloroquine, and (**H**) monensin. For all graphs **(B, D, F, H)**, each symbol represents the average PL pS1292–LRRK2 fluorescence intensity obtained from 100-150 cells per treatment group for each of three independent experiments. Statistical testing by two-way ANOVA with Tukey correction; ****denotes $p<0.0001$; ns denotes not significant.

4-HNE is a critical signaling mediator of LRRK2 kinase activity

LRRK2 kinase activity is provoked by membrane-damaging agents (*19, 20*) that cause lipid hydroperoxidation and accumulation of 4-HNE, a reactive aldehyde known to activate several kinases, including ERK, JNK, Src, and p38 MAPK (*25-28*). We examined whether exogenous 4-HNE could interact with and activate endogenous WT LRRK2 kinase activity. For this purpose, we devised a new PL assay, PL LRRK2-4-HNE, using antibodies that recognize 4-HNE and total LRRK2 to detect the formation of 4-HNE-LRRK2 adducts. When WT HEK293 cells were treated with a pathophysiological concentration of 4-HNE (100 μM for 1 hour), there was an increase in PL LRRK2–4-HNE signal, which was prevented by pre-treatment with NAC ($p<0.0001$; two-way ANOVA with Tukey correction) (***fig. S6***). This correlated with increased endogenous WT LRRK2 kinase activity as measured by PL pS1292-LRRK2 ($p<0.005$; two-way ANOVA with Tukey correction) (***fig. S7A, B***), and PL pT73(Rab10)-Rab10 ($p<0.005$; two-way ANOVA with Tukey correction (***fig. S7C, D***). NAC pre-treatment prevented the 4-HNE-induced increase in both PL pS1292-LRRK2 (***fig. S7A, B***), and PL pT73(Rab10)-Rab10 (***fig S7C, D***). These results demonstrate that exogenous 4-HNE can form adducts with and activate endogenous WT LRRK2.

To further examine the relationship between LRRK2–4-HNE adducts and LRRK2 kinase activity, WT HEK293 cells were treated with varying concentrations of 4-HNE (10 – 100 μM for 1 hour) and LRRK2–4-HNE adducts and LRRK2 activity were measured by PL. Increasing concentrations of 4-HNE caused parallel, dose-dependent increases in PL LRRK2–4-HNE and PL pS1292-LRRK2 signals (***Fig. 4A-D***) in WT HEK293 cells. In fact, within this concentration range, there was a highly significant linear relationship between the degree of LRRK2–4-HNE adduct formation and LRRK2 kinase activity ($p<0.005$; $R^2=0.99$) (***fig. S8***). Given that 4-HNE has a high

297 affinity for forming irreversible Michael adducts with cysteine residues, we also investigated
298 whether the cysteine mutants influence LRRK2-4-HNE adduct formation and 4-HNE-induced
299 kinase activity. Surprisingly, in LRRK2$^{C2024A+C2025A}$ HEK293 cells, 4-HNE treatment did not
300 increase PL LRRK2-4-HNE or PL pS1292-LRRK2 signals (***Fig 4A-D***). This suggests that, within
301 this concentration range, 4-HNE binds preferentially to the Cys2024 and Cys2025 residues of
302 LRRK2 in a cellular context.
303
304 To explore if LRRK2–4-HNE adduct formation occurs with endogenous generation of 4-HNE in
305 response to stimuli that activate LRRK2 kinase activity, we examined the effects of rotenone,
306 chloroquine, and monensin. Compared to vehicle, rotenone elicited an increase in PL LRRK2–4-
307 HNE signal in LRRK2$^{WT/WT}$ HEK293 ($p<0.0001$; two-way ANOVA with Tukey correction) and
308 RAW267.4 macrophages ($p<0.0001$; two-way ANOVA with Tukey correction) (***fig. S9)***. Co-
309 treatment with α-tocopherol, a compound that can protect against lipid hydroperoxidation (*42, 43*),
310 prevented the rotenone-induced increase in PL LRRK2–4-HNE signal and no signal was observed
311 in LRRK2$^{-/-}$ cells (***fig. S9)***. Similar to rotenone, both chloroquine and monensin treatment led to
312 an increase in PL LRRK2–4-HNE signal compared to vehicle ($p<0.0001$; two-way ANOVA with
313 Tukey correction) (***fig. S10***). Co-treatment with α-tocopherol prevented the chloroquine- and
314 monensin-induced increase in PL LRRK2–4-HNE and no signal was observed in LRRK2$^{-/-}$ cells
315 (***fig. S10***).
316
317 We previously showed there is 4-HNE accumulation and elevated LRRK2 kinase activity in
318 dopaminergic neurons of the substantia nigra (SN) in the rotenone rat model of PD (*9, 44, 45*).
319 Therefore, we investigated whether LRRK2–4-HNE adduct formation also occurred in this model.

320 As described (*45*), middle-aged rats were treated with rotenone for 7-10 days until they reached
321 behavioral endpoint, at which time they were euthanized for analysis. Rotenone treatment led to a
322 marked increase in PL LRRK2–4-HNE signal in SN dopamine neurons compared to vehicle ***(Fig.***
323 ***4E, G)***) ($p<0.01$; two tailed unpaired *t*-test with Welch's correction), thereby providing *in vivo*
324 relevance of LRRK2–4-HNE adduct formation. Together, these data demonstrate that the lipid
325 hydroperoxidation end-product, 4-HNE, may be a key signaling mediator in LRRK2 kinase
326 activation that links mitochondrial and endolysosomal stress to LRRK2 kinase activation.

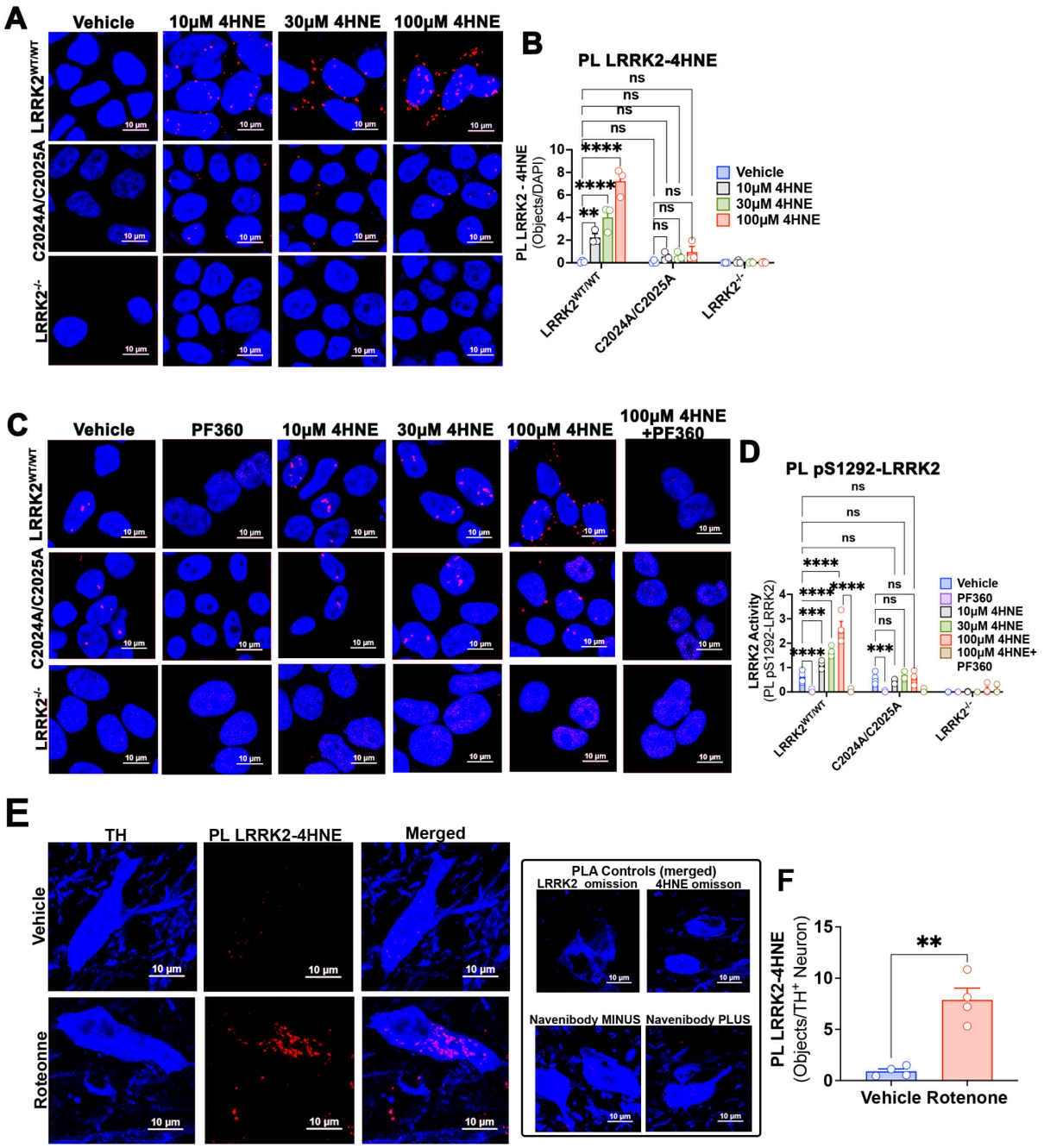

Figure 4. The lipid hydroperoxidation product 4-HNE interacts with LRRK2 and induces kinase activation. (**A**) PL between LRRK2 and 4-HNE (PL LRRK2–4-HNE) was used as an index of LRRK2-4-HNE adduct formation in LRRK2$^{WT/WT}$, C2024A/C2025A, and LRRK2$^{-/-}$ HEK293 cells. Exogenous 4-HNE treatment (10μM, 30μM, 100μM) led to a dose-dependent increase in PL LRRK2–4-HNE signal (red dots) in LRRK2$^{WT/WT}$ cells. 4-HNE treatment did not increase PL LRRK2–4-HNE signal in C2024A/C2025A and LRRK2$^{-/-}$ HEK293 cells. (**B**) Quantification of PL LRRK2-4-HNE. (**C**) 4-HNE-induced LRRK2 kinase activity was assessed by PL pS1292-LRRK2. Baseline kinase activity in LRRK2$^{WT/WT}$ and C2024A/C2025A cells was inhibited by the LRRK2 kinase inhibitor PF360 (1μM), and 4-HNE treatment dose-dependently increased PL pS1292-LRRK2 signal (red dots) in LRRK2$^{WT/WT}$ cells, but not in C2024A/C2025A cells. (**D**) Quantification of LRRK2 activity by PL pS1292–LRRK2 Objects/DAPI in HEK293 cells. For graphs **(B** and **D)**, each symbol represents the average signal from

100-150 cells per treatment group for each of three independent experiments. Statistical testing by two-way ANOVA with post-hoc Tukey correction. (**E**) LRRK2–4-HNE interaction was assessed via PL LRRK2–4-HNE (red dots) in TH^+ dopaminergic neurons (blue) in in the substantia nigra of rats treated with vehicle or rotenone. Rotenone treatment caused an increase in PL LRRK2–4-HNE in TH^+ dopaminergic neurons compared to vehicle treated rats. (**F**) Quantification of the PL LRRK2–4-HNE signal in dopamine neurons. Each symbol represents the average number of PL LRRK2–4-HNE objects/ TH^+ neuron from an individual animal with two sections of brain tissue stained per animal; N=4 animals per treatment group. Statistical testing by two-tailed unpaired *t*-test with Welch's correction. **denotes p<0.01; ***denotes p<0.0005; ****denotes p<0.0001; ns denotes not significant.

15-Lipoxygenase regulates LRRK2 kinase activity

Since 4-HNE forms adducts with LRRK2 and regulates its kinase activation, we explored the possible upstream sources of this reactive aldehyde. 4-HNE can be produced nonenzymatically when membrane lipids react directly with ROS; alternatively, it can be produced enzymatically as the end-product of 15-LO activity (*29, 30*). Our data demonstrate that α-tocopherol can prevent stimulus-induced PL LRRK2–4-HNE in an endogenous context, but it is unclear whether this is due to its ROS scavenging properties or its ability to inhibit 15-LO (*33*). We therefore used both genetic and pharmacological approaches to assess the role of 15-LO in producing the pool of 4-HNE that activates LRRK2. We utilized CRISPR/Cas9 gene-edited 15-LO knockout ($15\text{-}LO^{-/-}$) HAP1 cells and a novel, potent, and selective small molecule 15-LO inhibitor, CU-12991, that has an IC_{50} of 2.5 nM for inhibition of rotenone-induced 4-HNE production (***fig. S11***). In WT cells, rotenone elicited an increase in cellular 4-HNE, which was prevented by co-treatment with 20nM CU-12991 ($p < 0.0001$; two-way ANOVA with Tukey correction) ***(fig. S12A, B)***. There was no rotenone-induced 4-HNE accumulation in $15\text{-}LO^{-/-}$ cells, and CU-12991 had no effect in these cells ***(fig. S12A, B)***. Thus, in the absence of 15-LO activity, there was no rotenone-induced 4-HNE production.

We next explored whether 15-LO-derived 4-HNE mediates rotenone-induced LRRK2 activity. First, we assessed LRRK2–4-HNE adduct formation via PL LRRK2–4-HNE. Consistent with our

368 previous observations (***Fig. 4 and Fig. S9),*** rotenone increased the PL LRRK2–4-HNE signal
369 compared to the vehicle ($p<0.0005$; two-way ANOVA with Tukey correction), and this was
370 prevented by co-treatment with α-tocopherol (***Fig. 5A, B***). Strikingly, there was no rotenone-
371 induced PL LRRK2–4-HNE signal in 15-LO$^{-/-}$ cells (***Fig. 5A, B***). Next, we assessed kinase
372 activation by both autophosphorylation (***Fig. 5C, D***) and substrate phosphorylation (***fig. S12C, D).***
373 In WT cells, rotenone increased PL pS1292-LRRK2 signal ($p<0.0001$; two-way ANOVA with
374 Tukey correction) (***Fig. 5C, D***) and PL pT73(Rab10)-Rab10 signal ($p<0.0001$; two-way ANOVA
375 with Tukey correction) (***fig. S12C, D)***. Interestingly, 15-LO inhibition by CU-12991 mitigated the
376 rotenone-induced increase in PL pS1292-LRRK2 (***Fig. 5C, D***) and PL pT73(Rab10)-Rab10 (***fig.***
377 ***S12C, D)***, but did not reduce LRRK2 kinase activity below basal levels (***Fig. 5C, D***). In contrast,
378 PF360 treatment completely abolished both basal and rotenone-induced kinase activity (PL
379 pS1292-LRRK2, ***Fig. 5C, D***) (PL pT73(Rab10)-Rab10, ***fig. S12C, D***).
380
381 Consistent with our results using CU-12991, in 15-LO$^{-/-}$ cells there was no rotenone-induced PL
382 pS1292-LRRK2 (***Fig. 5C, D***) or PL pT73(Rab10)-Rab10 (***fig. S12C, D***), although basal kinase
383 activity was preserved. Importantly, CU-12991 did not impact LRRK2 activity in 15-LO$^{-/-}$ cells
384 ***(Fig 5C, D*** and ***fig. S12C, D***). Furthermore, to ensure CU-12991 was not directly interfering with
385 4-HNE, we treated cells with exogenous 4-HNE and found that induced kinase activity was
386 unaffected by CU-12991 (***fig. S13).***
387
388 To ensure that the stimulatory effect of 15-LO on LRRK2 kinase activity was due to its production
389 of 4-HNE, we treated cells with exogenous 4-HNE (***Fig. 5E, F***). In both WT and 15-LO$^{-/-}$ cells, 4-
390 HNE elicited an increase in PL pS1292-LRRK2 signal ($p<0.005$; two-way ANOVA with Tukey

391 correction), which was prevented by treatment with NAC (***Fig 5E, F***). Thus, the effects of
392 pharmacological inhibition or genetic deletion of 15-LO on LRRK2 kinase activity can be
393 overcome by exogenous 4-HNE. Collectively, these results suggest that 4-HNE generated by 15-
394 LO forms adducts with LRRK2, leading to its hyperactivation. Therefore, LRRK2 kinase
395 activation is specifically regulated by the 4-HNE produced by 15-LO as an end-product of lipid
396 hydroperoxidation.
397
398 Accumulation of 4-HNE in the SN of PD post-mortem human brain tissue has been recognized for
399 30 years (*46*); however, the functional role of 15-LO-derived 4-HNE in PD has yet to be explored.
400 Therefore, we assessed 4-HNE levels in patient-derived lymphoblastoid cell lines (LCLs) derived
401 from healthy control subjects, G2019S-LRRK2 PD patients, and iPD patients. Relative to healthy
402 controls, basal 4-HNE was elevated in LCLs derived from subjects with iPD as well as subjects
403 harboring a G2019S mutation ($p < 0.0001$ for both iPD and G2019S compared to healthy controls;
404 two-way ANOVA with Tukey correction) ***(Fig. 5H)***. The elevated 4-HNE signal in the iPD and
405 G2019S PD subjects was reduced to healthy control levels by treatment with CU-12991 ($p <$
406 0.0001 for both iPD and G2019S; two-way ANOVA with Tukey correction two-way ANOVA with
407 Tukey correction) ***(Fig. 5H)***. This suggests that 15-LO is responsible for the pathological
408 accumulation of 4-HNE observed in G2019S and iPD patient samples.

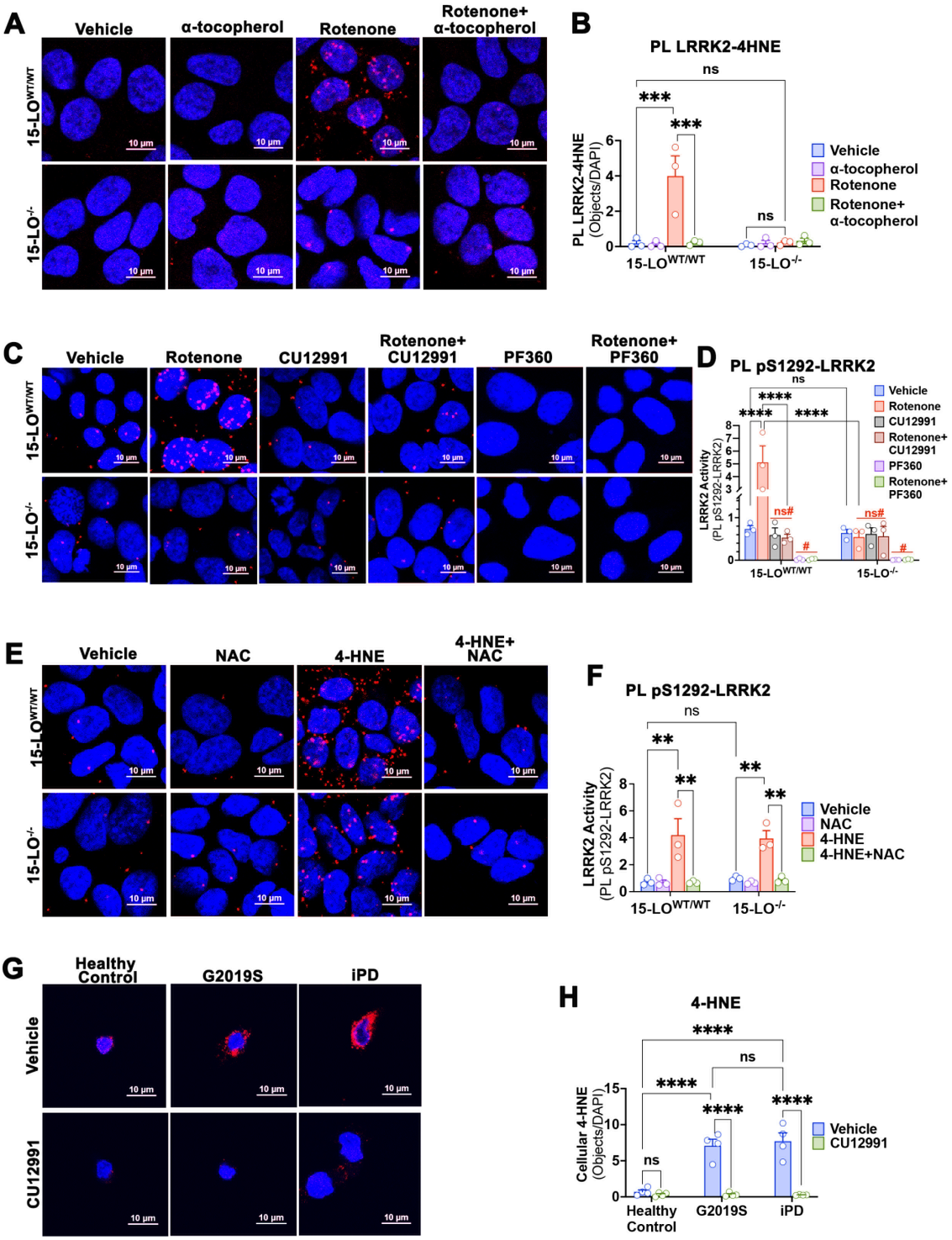

Figure 5. 15-LO-derived 4-HNE is a key mediator of LRRK2 hyperactivation. (**A**) Rotenone-induced endogenous LRRK2–4-HNE adduct formation was assessed by PL LRRK2-4-HNE in 15-LO$^{WT/WT}$ and 15-LO$^{-/-}$ HAP1 cells. Rotenone treatment promoted an increase in PL LRRK2-4-HNE signal that was prevented by α-tocopherol in 15-LO$^{WT/WT}$, and not observed in 15-LO$^{-/-}$ cells. (**B**) Quantification of PL LRRK2-4-HNE. (**C**) Rotenone-induced LRRK2 kinase activity was assessed by

PL pS1292-LRRK2. Rotenone increased PL pS1292-LRRK2, an effect that was that was mitigated by cotreatment with the 15-LO inhibitor, CU-12991, and completely prevented by PF360. 15-LO$^{-/-}$ cells had a normal basal PL pS1292 – LRRK2 signal, which was not further increased by rotenone or affected by CU-12991. (**D**) Quantification of LRRK2 activity by PL pS1292-LRRK2. (**E**) 4-HNE (100μM) treatment led to an increase in PL pS1292-LRRK2 signal in both 15-LO$^{WT/WT}$ and 15-LO$^{-/-}$ cells. This was prevented by pretreatment with 250μM NAC. (**F**) Quantification of LRRK2 activity by PL pS1292-LRRK2. For graphs **(B, D,** and **F)**, each symbol represents the average signal from 100-150 cells per treatment group for each of three independent experiments. Statistical testing by two-way ANOVA with post-hoc Tukey correction. (**G**) Cellular 4-HNE signal in LCLs derived from healthy control subjects, G2019S mutation carriers, and iPD patients. The increased 4-HNE signal in G2019S and iPD LCLs was reduced to healthy control levels by CU-12991. (**H**) Quantification of 4-HNE. Each symbol represents an individual donor line. 4-HNE signal was taken from 90-120 cells/line; 4 donor lines per group. Statistical testing by two-way ANOVA with post-hoc Tukey correction. **denotes p<0.005; *** denotes p<0.0005; ****denotes p<0.0001; ns denotes not significant. For panel D, red symbols indicate additional statistical testing by one-way ANOVA, examining each genotype (15-LO$^{WT/WT}$ and 15-LO$^{-/-}$) separately. ns# denotes not significant compared to vehicle-treated cells; # denotes p< 0.05 compared to vehicle-treated or CU-12991-treated cells.

Next we investigated whether 15-LO-derived 4-HNE was responsible for LRRK2–4-HNE adduct formation elicited by other known LRRK2 activators: chloroquine, monensin, or rotenone. Consistent with our results in HEK cells ***(fig. S9, fig. S10)***, in WT RAW264.7 macrophages chloroquine, monensin, and rotenone each elicited an increase in PL LRRK2-4-HNE signal (***Fig. 6A, B***). As observed in 15-LO$^{-/-}$ HAP1 cells (***Fig. 5A, B)***, 15-LO inhibition with CU-12991 prevented the formation of rotenone-induced LRRK2–4-HNE adducts (***Fig. 6A, B)*** in WT RAW264.7 macrophages. Similarly, CU-12991 co-treatment prevented chloroquine- and monensin-induced PL LRRK2-4-HNE signal in WT RAW264.7 macrophages (***Fig. 6A, B)***. Under the same conditions, chloroquine, monensin, and rotenone each significantly increased PL pS1292-LRRK2 signal in WT RAW264.7 macrophages (***Fig. 6C, D***). Strikingly, CU-12991 co-treatment completely prevented rotenone-, chloroquine-, and monensin-induced PL pS1292-LRRK2 signal (***Fig. 6C, D).*** As an orthogonal approach to measure LRRK2 kinase activity, we assessed substrate phosphorylation via pT73-Rab10 western blot. Chloroquine, monensin, and rotenone each led to an increase in pT73-Rab10, which was prevented by co-treatment with CU-12991 (***fig. S14***). Thus,

449 using genetic and pharmacological approaches and three independent LRRK2 activity assays (PL
450 pS1292–LRRK2, pThr-73-Rab10 western blot, and PL pT73(Rab10)-Rab10), our results indicate
451 that endogenous stimulated LRRK2 activity is regulated by 15-LO.
452
453 Although both 15-LO and 12-lipoxygenase (12-LO) can participate in lipid peroxidation, 15-LO
454 activity is the predominant source of 4-HNE formation. The initial step in this enzymatic pathway
455 (for both 15-LO and 12-LO) produces their respective hydroperoxy lipid metabolites: 15(S)-
456 HpETE for 15-LO and 12(S)-HpETE for 12-LO (*29, 30*). A subsequent intramolecular
457 rearrangement of 15(S)-HpETE, but not 12(S)-HpETE, produces 4-HNE (*47*). To further validate
458 the 15-LO pathway and subsequent 4-HNE formation as a regulator of LRRK2 kinase activity, we
459 treated WT RAW264.7 macrophages with either 15(S)-HpETE or 12(S)-HpETE and assessed
460 endogenous LRRK2 kinase activation by PL pS1292-LRRK2. 12(S)-HpETE treatment (0.25 – 25
461 μM) did not increase PL pS1292–LRRK2 signal (***Fig. 6E, F***); however, 15(S)-HpETE dose-
462 dependently increased PL pS1292–LRRK2 signal ($p<0.0001$; two-way ANOVA with Tukey
463 correction) (***Fig. 6E, F*)**. NAC pre-treatment prevented 15(S)-HpETE-induced PL pS1292–
464 LRRK2 signal (***Fig. 6E, F***). Together, these results indicate that LRRK2 kinase activation was
465 driven by 15(S)-HpETE rearrangement to 4-HNE.
466
467 To determine the PD relevance of 15-LO-regulated LRRK2 activity, we next investigated if
468 LRRK2 activity was elevated in G2019S PD and iPD patient-derived LCLs. Relative to healthy
469 controls, there was elevated PL pS1292-LRRK2 in both G2019S ($p < 0.0001$; two-way ANOVA
470 with Tukey correction) and iPD LCLs ($p < 0.005$; two-way ANOVA with Tukey correction) that
471 was completely abolished by PF360 (***Fig. 6G, H)***. Strikingly, CU-12991 reduced pathologically
472 hyperactive LRRK2 kinase activity in both G2019S and iPD LCLs back to basal healthy control

473 levels but did not completely inhibit LRRK2 activity (***Fig. 6G, H***). Collectively, these data provide
474 strong evidence that 15-LO activity regulates pathologically elevated endogenous LRRK2 kinase
475 activity through the enzymatic production of 4-HNE and its subsequent adduct formation with
476 LRRK2.

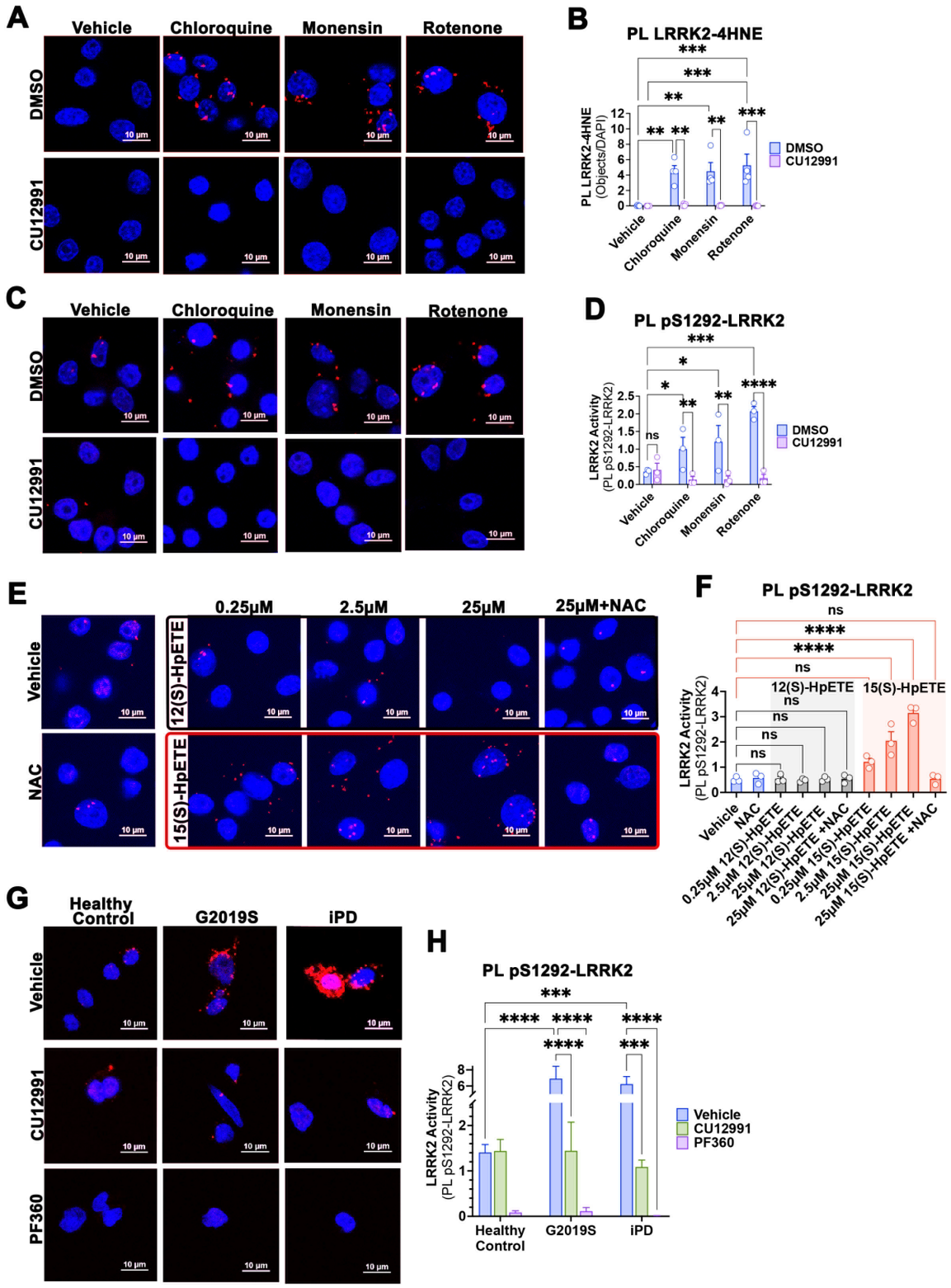

Figure 6. 15-LO activity regulates stimulated LRRK2 kinase activity via 4-HNE. (**A**) LRRK2-4-HNE adduct formation was assessed by PL LRRK2-4-HNE in LRRK2$^{WT/WT}$ RAW264.7 macrophages. Chloroquine, monensin, and rotenone led to an increase PL LRRK2-4-HNE signal (red dots). The

increase in PL LRRK2-4-HNE signal was prevented by cotreatment with CU-12991. (**B**) Quantification of PL LRRK2-4-HNE. (**C**) Chloroquine, monensin, and rotenone-induced kinase activity was assessed by PL pS1292-LRRK2 in LRRK2$^{WT/WT}$ RAW264.7 macrophages. Chloroquine, monensin and rotenone caused increased PL pS1292-LRRK2 signal (red dots) which was prevented by cotreatment with the 15-LO inhibitor, CU-12991. (**D**) Quantification of LRRK2 activity by PL pS1292-LRRK2. (**E**) LRRK2$^{WT/WT}$ RAW264.7 macrophages were treated with either 12(S)-HpETE (top panel, black outline) or 15(S)-HpETE (bottom panel, red outline) and kinase activity was measured by PL pS1292-LRRK2. 12(S)-HpETE did not increase PL pS1292-LRRK2 signal above baseline (red dots). 2.5μM and 25μM 15(S)-HpETE led to an increase in PL pS1292-LRRK2 signal relative to vehicle. Cotreatment with NAC prevented the increase in PL pS1292-LRRK2 signal elicited by 25μM 15(S)-HpETE. (**F**) Quantification of LRRK2 activity by PL pS1292–LRRK2. For each graph (**B**, **D**, and **F**), each symbol represents the average number of PL LRRK2-4-HNE Objects/DAPI or PL pS1292-LRRK2 Objects/DAPI obtained from 100-150 cells per treatment group for each of 3-4 independent experiments. Statistical testing by two-way ANOVA with post-hoc Tukey correction. (**G**) LRRK2 activity measured by PL pS1292-LRRK2 in LCLs derived from healthy control subjects, G2019S mutation carriers, and iPD patients. The increased PL pS1292-LRRK2 signal in G2019S and iPD LCLs was reduced to healthy control basal levels by CU-12991 and completely blocked by PF360. (**H**) Quantification of LRRK2 activity by PL pS1292-LRRK2 Objects/DAPI was taken from 90-120 cells/line; 4 donor lines per group. Statistical testing by two-way ANOVA with post-hoc Tukey correction. * denotes $p<0.05$; **denotes $p<0.005$; *** denotes $p\leq0.0005$; **** denotes $p<0.0001$; ns denotes not significant.

The ability of 15-LO to hydroperoxidate membrane phospholipids depends on its association with the small scaffolding protein, phosphatidylethanolamine-binding protein (PEBP1) (*48*). Typically, PEBP1 is in complex with RAF1 kinase; however, upon phosphorylation, it is liberated and interacts with new proteins (*49*), including 15-LO. In the unbound state, 15-LO prefers as substrates free fatty acids, not those incorporated into membranes. However, when complexed with PEBP1, its substrate preference switches to omega-6 PUFAs incorporated into membrane phosphatidylethanolamines (*48, 50*), and omega-6 PUFA hydroperoxidation results in the production of 4-HNE. We therefore explored the interaction between PEBP1 and 15-LO in a system (rotenone-treated RAW264.7 macrophages) where endogenous 4-HNE production is stimulated with resultant LRRK2 kinase activation. Quantitative confocal immunofluorescence staining revealed that rotenone treatment markedly increased the colocalization of the PEBP1 and 15-LO ($p < 0.005$; two tailed unpaired *t*-test with Welch's correction) (***Fig. 7A, B***). Using a complementary approach, we developed a PL assay that detects the interaction between PEBP1

516 and 15-LO (PL PEBP1–15-LO). Similar to our colocalization results, rotenone-induced a strong
517 PL PEBP1–15-LO signal compared to vehicle (***Fig. 7C, D)***.
518
519 We also examined if this occurred *in vivo* in the rotenone rat model of PD (***Fig. 7E, F***). Analogous
520 to our findings in macrophages, there was an increase in PL PEBP1–15-LO signal in dopaminergic
521 neurons in rotenone-treated rats compared to vehicle ($p < 0.0005$; two-tailed unpaired *t*-test with
522 Welch's correction) (***Fig. 7E, F***). To investigate if this was relevant in the human disease, we
523 sought to determine if PL PEBP1-15-LO was increased in LCLs derived from G2019S PD and
524 iPD patients compared to healthy controls. Indeed, there was an elevated PL PEBP1–15-LO signal
525 in LCLs derived from G2019S ($p < 0.05$; one-way ANOVA with Tukey correction) and iPD
526 ($p=0.005$; one-way ANOVA with Tukey correction) patients compared to healthy controls (***Fig.***
527 ***7G, H***). Thus, using complementary approaches in multiple model systems and PD patient
528 samples, the data demonstrate that under conditions generating endogenous 4-HNE and
529 stimulating LRRK2 kinase activity, there is an enhanced association between 15-LO and PEBP1.
530
531
532

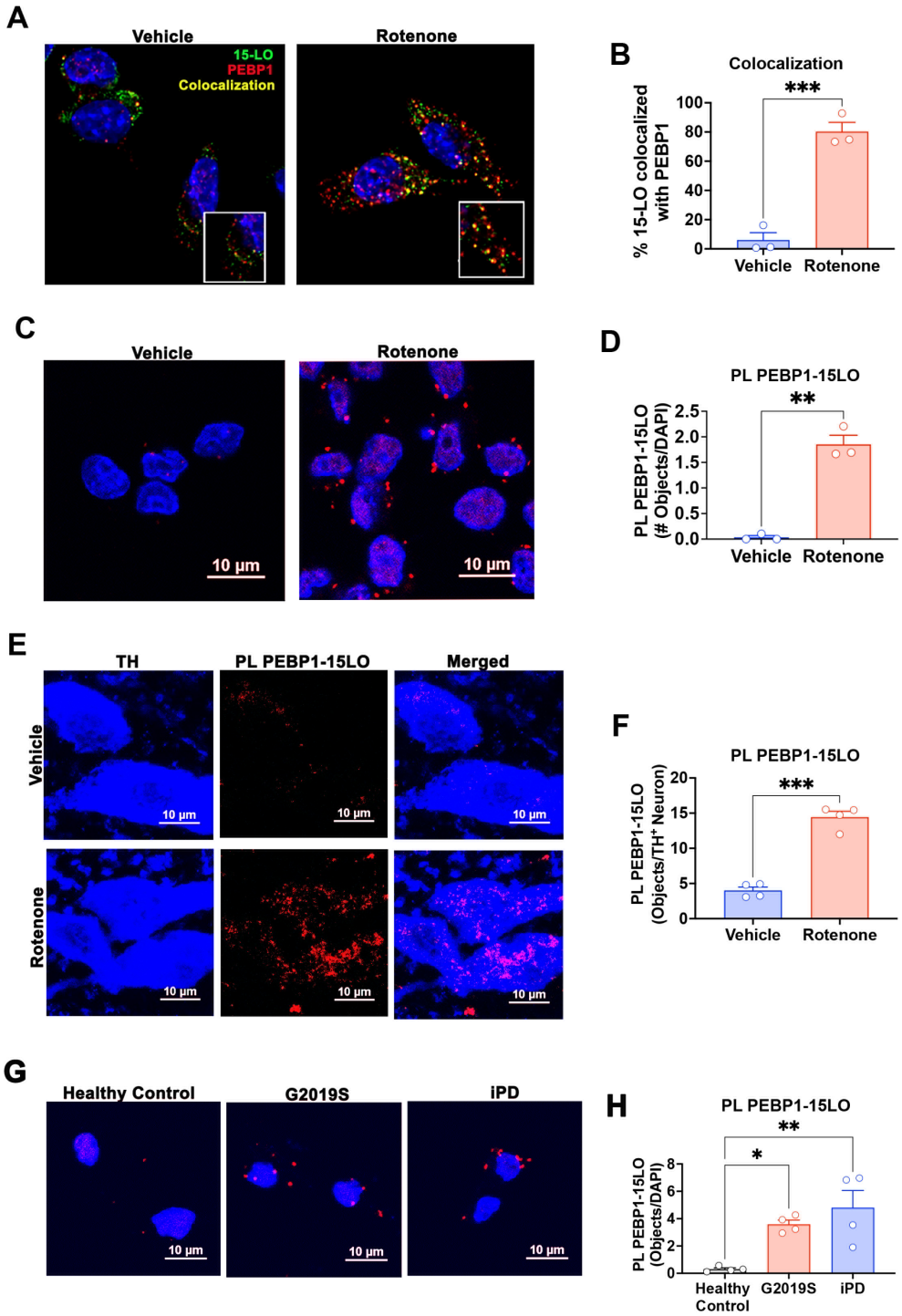

Figure 7. PEBP1 and 15-LO interaction is increased in the rotenone model and patient derived samples. (**A**) Immunofluorescent staining for 15-LO (green), PEBP1 (red), and their colocalization (yellow) in LRRK2$^{WT/WT}$ RAW264.7 macrophages. Rotenone led to an increase in overlap between 15-LO and PEPB1 relative to vehicle. Inset is 200X zoom. (**B**) Quantification of the % overlap of 15-LO and PEBP1 objects/Total Number of 15-LO Objects. Each symbol represents the average % overlap of 15-LO and PEBP1 objects/Total Number of 15-LO Objects obtained from 100-150 cells per treatment group for each of three independent experiments. Statistical testing by two tailed unpaired *t*-test with Welch's correction. *** denotes p<0.001 (**C**) PL between PEBP1 and 15-LO was used as

542 an index for PEPB1–15-LO interaction in LRRK2$^{WT/WT}$ RAW264.7 macrophages. Rotenone treatment
543 led to an increase in PL PEBP1–5-LO signal (red dots) compared to vehicle. (**D**) Quantification of PL
544 PEBP1–15-LO . Each symbol represents the average number of PL PEBP1–15-LO Objects/DAPI
545 obtained from 100-150 cells per treatment group for each of three independent experiments. Statistical
546 testing by two tailed unpaired *t*-test with Welch's correction. ** denotes $p<0.01$ (**E**) PEBP1–15-LO
547 interaction was assessed via PL PEBP1–15-LO (red dots) in TH^+ dopaminergic neurons (blue) in the
548 substantia nigra of rats treated with vehicle or rotenone. Rotenone treatment caused an increase in
549 PL PEBP1–15-LO in TH^+ dopaminergic neurons compared to vehicle-treated rats. (**F**) Quantification
550 of the PL PEBP1–15-LO signal in dopamine neurons. Each symbol represents the average number of
551 PL PEBP1–15-LO HNE objects/ TH^+ neuron from an individual animal with two sections of brain tissue
552 stained per animal; N=4 animals per treatment group. Statistical testing by two-tailed unpaired *t*-test
553 with Welch's correction.***denotes $p<0.0005$. (**G**) PL PEBP1–15-LO was assessed in LCLs derived
554 from healthy control subjects, G2019S mutation carriers, and iPD patients. There was an increase in
555 PL PEBP1–15-LO signal in G2019S and iPD derived LCLs relative to healthy control. (**H**)
556 Quantification of PL PEBP1–15-LO Objects/DAPI. Each symbol represents the average number of PL
557 PEBP1–15-LO Objects/DAPI taken from 90-120 cells/line; 4 donor lines per group. Statistical testing
558 by one-way ANOVA with post-hoc Tukey correction * denotes $p<0.05$; ** denotes $p\leq0.005$.
559

560

561 **DISCUSSION**

562

563 Pathogenic mutations in *LRRK2* that cause elevated kinase activity are predominantly driven by
564 altered kinetics, altered GTP hydrolysis, or enhanced substrate specificity (*8, 12, 13, 51*). Although
565 each pathogenic mutation can increase LRRK2 kinase activity, they do so in distinct ways,
566 highlighting the complexity of LRRK2 activation. When assessing kinase activity, cellular *in situ*
567 assays have advantages over *in vitro* kinase assays, as the cellular context is important for LRRK2
568 activation (*6*). Upstream signaling events may be critical for understanding how and where
569 endogenous WT LRRK2 activation occurs and what substrates are involved. In this work, we
570 aimed to elucidate what regulates pathologically elevated LRRK2 kinase activity. To strengthen
571 our conclusions, kinase activity was assessed using three complementary approaches: (i) PL
572 pS1292-LRRK2, (ii) pT73-Rab10 western blot and (iii) PL pT73(Rab10)-Rab10, each of which
573 yielded similar results.

574

575 In our studies, treating cells with a physiological concentration of H_2O_2 led to a rapid increase in
576 LRRK2 activation within 5-10 minutes, which was prevented by quenching with NAC. This
577 suggests that LRRK2 itself may be redox-sensitive. Similarly, various cellular perturbations that
578 promote LRRK2 activation, such as mitochondrial stress (rotenone), lysosomal dyshomeostasis
579 (chloroquine), and vesicular trafficking deficits (monensin) have also been shown to result in redox
580 damage (*21, 22, 35, 36, 52-54*). Here we demonstrated that these perturbations can stimulate 4-
581 HNE accumulation and subsequent adduct formation with LRRK2 (***fig. S15)***.

582

583 The dynamics of the kinase domain have a strong influence on the kinase activation state of
584 LRRK2 (*12, 13*). We found that Cys2024/2025 in the kinase activation loop are important residues

585 for stimulated LRRK2 activation. Recent work by others has also suggested that these cysteine
586 residues may be important for kinase activation (*37*); however, they used *in vitro* kinase assays and
587 experiments (*37*), whereas we maintained an endogenous cellular context and used multiple
588 complementary assays to support our conclusions. We found that while the cysteine-to-alanine
589 mutations preserved basal kinase activity, stimulated LRRK2 activity was completely prevented.
590 The fact that LRRK2 bearing these cysteine-to-alanine mutations had little, if any, propensity to
591 form adducts with 4-HNE suggests that 4-HNE preferentially targets these solvent-exposed
592 Cys2024/2025 residues. It is important to note that the Cys2024/2025 to Ala mutants are not
593 "kinase-dead"; they retain normal basal activity but simply cannot be further activated. A previous
594 study postulated that the development of LRRK2 kinase inhibitors directed towards Cys2024 and
595 Cys2025 may hold therapeutic benefit (*55*). Our study supports this hypothesis and indicates these
596 residues are critical for LRRK2 hyperactivation. It is unlikely that redox stress causes
597 Cys2024/2025 to form an intramolecular disulfide bridge in monomeric LRRK2, as disulfide
598 bridge formation between vicinal cysteine residues is an extremely rare biological phenomenon
599 (*56*). Whether intermolecular disulfide bonds involving these cysteine residues might occur in
600 higher-order oligomeric species of LRRK2 (*57*) is unknown.
601
602 LRRK2 activation has been shown to be associated with damaged membranes, especially in the
603 endolysosomal system (*20-23, 35*). As noted, endolysosomal impairment and mitochondrial stress
604 lead to the formation of the lipid peroxidation product 4-HNE. This raises the possibility that this
605 reactive aldehyde may be important in LRRK2 activation and might provide a link between
606 membrane damage and LRRK2 activation. Given that 4-HNE is known to activate other kinases
607 (*25-28*), there is precedent for this idea. Indeed, we found that treatment of cells with exogenous

608 4-HNE led to dose-dependent increases in LRRK2-4-HNE adduct formation and LRRK2 kinase
609 activation – with a strong linear correlation between the two. Similarly, other LRRK2 activating
610 stimuli (rotenone, chloroquine, monensin, and H_2O_2), which lead to the endogenous accumulation
611 of 4-HNE, also resulted in LRRK2-4-HNE adduct formation. Interestingly, Rab GTPases, which
612 have been shown to activate LRRK2 (*58, 59*), may also be modified by 4-HNE (*60*). Furthermore,
613 STING pathway activation, which leads to lipid hydroperoxidation (*61*), plays a role in the
614 activation of LRRK2 at damaged lysosomes (*23*). As such, 4-HNE formation appears to be a
615 convergent event shared by these seemingly disparate LRRK2 activating stimuli. Thus, 4-HNE
616 may be a final common regulator of LRRK2 kinase activation.
617
618 Levels of 4-HNE and 4-HNE protein adducts are elevated in PD patients compared to healthy
619 controls (*46, 62*). 4-HNE can be formed nonenzymatically or enzymatically through the 15-LO
620 pathway (*29, 30*). Therefore, we explored whether 15-LO activity regulates 4-HNE production,
621 LRRK2–4-HNE adduct formation, and LRRK2 kinase activation. Remarkably, 15-LO knockout
622 or 15-LO inhibition with CU-12991 potently blocked rotenone-stimulated 4-HNE production,
623 LRRK2-4-HNE adducts, and LRRK2 kinase hyperactivation but did not inhibit basal kinase
624 activity. Moreover, the 15-LO specific metabolite 15(S)-HpETE, which undergoes subsequent
625 intramolecular rearrangement to form 4-HNE, dose-dependently increased LRRK2 activity.
626 Importantly, we demonstrated in patient-derived iPD and G2019S PD LCLs that there are elevated
627 basal 4-HNE levels and LRRK2 kinase activity that could be reduced to healthy control levels by
628 inhibiting 15-LO with CU-12991. Thus, we conclude that the specific end-product of 15-LO
629 activity, 4-HNE, is sufficient for endogenous pathologic LRRK2 activity (***fig. S15)***.
630

631 Normally, 15-LO prefers to hydroperoxidate free fatty acids, not those incorporated into
632 membranes. However, its substrate specificity is regulated by interaction with PEBP1 (*48*). When
633 15-LO is in complex with PEBP1, it acquires the ability to oxygenate membrane phospholipids
634 (*48*), which ultimately results in the formation of 4-HNE. In this regard, we found that rotenone
635 led to an increase in the association of 15-LO with PEBP1 *in vitro* and *in vivo*. We found that
636 stimuli that increase endogenous WT LRRK2 kinase activity also (i) enhance the PEBP1–15-LO
637 interaction, (ii) increase 4-HNE production, and (iii) cause LRRK2-4-HNE adducts to form (***fig.***
638 ***S15)***. Strikingly, this association was observed in both G2019S PD and iPD patient-derived
639 samples, confirming the relevance of this mechanism to human disease. These data suggest that
640 the increase in 15-LO–PEBP1 interaction leads to elevated 4-HNE levels at specific membranes,
641 which in turn promotes the hyperactivation of LRRK2. The fact that this sequence of events is
642 demonstratable in G2019S PD and iPD patient-derived samples provides strong evidence for the
643 15-LO pathway as a key contributor to PD pathogenesis through the regulation of LRRK2 activity.
644

645 Our study has some limitations. We acknowledge that while our data strongly implicates cysteine
646 residues 2024 and 2025 in the redox-dependent activation of LRRK2, we did not show directly
647 that they undergo a specific 4-HNE post-translational modification. Additionally, we have not
648 determined the subcellular localization of LRRK2 activation in response to these stimuli. It will
649 be important to determine if LRRK2 activation and LRRK2–4-HNE interaction occur in one
650 specific cellular compartment, or if it is dependent on the location of the inciting insult (*e.g.*,
651 lysosomes, mitochondria).
652

653 In summary, we have defined a new mechanism of cellular perturbation-induced LRRK2 kinase
654 activation. Our data demonstrate that LRRK2 is a redox-sensitive kinase and Cys2024/2025 are
655 critical for stress-induced stimulation of kinase activity. Moreover, we found that seemingly
656 disparate LRRK2 activating stimuli (chloroquine, H_2O_2, monensin, and rotenone), each with a
657 different proximal mechanism of action, activate LRRK2 through a convergent redox-dependent
658 mechanism that is mediated by the lipid hydroperoxidation end-product, 4-HNE, which forms
659 adducts with LRRK2. Further, 15-LO, the enzymatic source of 4-HNE**,** was identified as the
660 upstream mediator of stimulated LRRK2 kinase activation (***fig. S15)***. These results suggest that
661 15-LO inhibitors or drugs that otherwise reduce lipid hydroperoxidation may provide a new
662 therapeutic avenue to target the LRRK2 pathway in PD. Moreover, the fact that inhibition of 15-
663 LO prevented stimulus-induced LRRK2 kinase hyperactivation in cell lines, and disease-
664 associated hyperactivity in LCLs, without impacting basal kinase activity, may allow therapeutic
665 modulation of LRRK2 while avoiding on-target liabilities.
666
667
668

669 # MATERIALS AND METHODS

670

671 **Study Design**

672 This study was designed to explore the mechanism(s) that drive endogenous WT LRRK2 kinase
673 activation. To this end we used CRISPR/Cas9 gene-edited HEK293 cells, CRISPR/Cas9 gene-
674 edited HAP1 cells, as well as RAW264.7 macrophages, patient-derived LCLs, and an *in vivo*
675 rotenone rat model of PD to explore what physiological players regulate LRRK2 activation. To
676 enhance scientific rigor, we generally used orthogonal approaches to support each conclusion.
677 Furthermore, as target validation of 15-LO, specifically, 15-LO derived 4-HNE, being upstream
678 LRRK2 activation, we employed a specific and highly potent pharmacological inhibitor and
679 genetic knockout approaches to support key findings. To ensure clinical relevance and translational
680 potential, key results were confirmed in patient-derived LCLs and in an *in vivo* model of PD. All
681 *in vitro* experiments were replicated independently at least three times and performed by multiple
682 experimenters. *In vivo* experiments were conducted using a single cohort of rats that were assigned
683 randomly to treatment group.

684

685 **Cell Culture**

686 HEK293 cells and RAW264.7 macrophages were cultured in DMEM/F12 (cat:11320082, Thermo
687 Fisher) supplemented with 10% fetal bovine serum (FBS) and penicillin-streptomycin (pen-strep).
688 15-LO$^{WT/WT}$ and CRISPR/Cas9 gene-edited 15-LO$^{-/-}$ HAP1 cells were purchased from Horizon (
689 HZGHC007334c00) and cultured in IMDM (cat: 30-2005, ATCC) supplemented with 10% FBS
690 and pen-strep. Cells were maintained at 37°C and 5% CO_2. CRISPR/Cas9 gene-edited HEK293
691 cells were generated as previously described (*9*). LRRK2$^{-/-}$ (sc-6004) and LRRK2$^{WT/WT}$ (parental)
692 (sc-6003) RAW264.7 macrophages were obtained from ATCC. Cell passage number did not

693 exceed 20 for HEK293 or RAW264.7 macrophages. Cells were plated on poly-d-lysine coated
694 coverslips in a 24-well plate or 16-well Nunc Lab Tek chamber slides (cat: 178599, Thermo
695 Fisher). Details for reagents used for cell treatments can be found in Table S1. For H_2O_2, 4-HNE,
696 12(S)-HpETE, and 15(S)-HpETE treatments, DMEM/F12 supplemented with 5% fetal bovine
697 serum (FBS) and penicillin-streptomycin (pen-strep) was used.
698
699 Patient-derived lymphoblastoid cell lines were obtained from the NINDS Coriell Biorepository
700 through an MTA and sample ID numbers may be found in Table S2. Cells were maintained in
701 RPMI medium GlutaMAX supplement (cat: 61870127, Thermo Fisher Scientific) with 15% FBS
702 and pen-strep. Cells were plated on poly-d-lysine coated coverslips in a 24-well plate or 16-well
703 Nunc Lab Tek chamber slides (cat: 178599, Thermo Fisher) and attached by light centrifugation
704 at 690 x g at room temperature. Cells were passaged every 3 days and did not exceed 20 passages.
705
706 *CRISPR/Cas9 gene edited HEK293 cells (C2024A, C2025A, C2024A/C2025A)*
707 $LRRK2^{C2024A/C2024A}$, $LRRK2^{C2025A/C2025A}$ and double cysteine mutants were created in-house. A
708 guide RNA targeting exon 41 of the LRRK2 gene (5'- CTCAGTACTGCTGTAGAATG-3') was
709 commercially synthesized (ThermoFisher) and used to form ribonucleoprotein (RNP) complexes
710 when combined with recombinant Cas9 protein (New England Biolabs). Ribonucleoprotein
711 complexes were formed using the method of Kouranova[49]. RNP complexes were formed by
712 incubating the recombinant Cas9 protein and guide RNA at 1:1 mass ratio (1: 4.6 molar ratio of
713 the Cas9 protein to sgRNA) at 37°C for 5 min. RNPs were delivered to HEK293 cells using
714 Transit-X2 (Mirius) transfection reagent as described by the manufacturer. Single stranded repair
715 templates specific to the C2024 or C2025 residues were included in the transfection reactions to

716 facilitate the cysteine to alanine conversion by homologous recombination. The double mutant
717 C2024A/C2025A was generated in a similar fashion using the repair template specific to the
718 double mutation. Transfected cells were collected and enriched by FACS sorting. Sorted cells
719 were grown and expanded for PCR and DNA sequencing analyses. All clones generated by these
720 methods were sequenced on both strands to confirm their identity. Protein expression – or lack
721 thereof – was confirmed by western blotting. Using the same technology, $LRRK2^{G2019S/G2019S}$,
722 $LRRK2^{R1441G/R1441G}$, $LRRK2^{-/-}$ cells were created. Details for CRISPR/Cas9 reagents can be found
723 in Table S3.

724

725 **Dihydroethidium (DHE) Staining**

726 DHE staining was performed as described previously (*44*). A 3 mM stock solution of DHE (cat:
727 D11347, Thermo Fisher Scientific) was reconstituted in DMSO and stored at -20°C in single use
728 aliquots. Prior to use, the DHE stock solution was thawed, protected from light, and diluted in cell
729 culture media to reach a final concentration of 3μM DHE. Old media was aspirated and replaced
730 with the fresh media containing 3μM DHE. Cells were incubated for 20 minutes at 37°C and 5%
731 CO_2, protected from light. Cells were then gently washed with phosphate buffer saline (PBS) at
732 room temperature for 5 minutes and then fixed with 4% paraformaldehyde (PFA) (cat:15710-S,
733 Electron Microscopy Science) for 20 minutes. Following fixation, cells underwent three 10-minute
734 washes in PBS. Coverslips were mounted on glass slides (cat: 22-037-246, Fisher Scientific) using
735 gelvatol mounting medium (see (*34*) for recipe).

736

737

738

739 **Immunofluorescence**

740 Cells were fixed in 4% paraformaldehyde in phosphate buffer saline (PBS) for 20 minutes at room
741 temperature, followed by three 10-minute washes in PBS on a shaker. Cells were blocked and
742 permeabilized in 10% normal donkey serum (NDS) + 0.02% triton-x in PBS for 1 hour at room
743 temperature on a shaker. After blocking/permeabilization, cells underwent three washes in PBS
744 and then were incubated in primary antibody (Table S4, for antibody details) in PBS containing
745 1% NDS overnight at 4ºC on a shaker. The following day, cells underwent three 10-minute washes
746 in PBS and were incubated in secondary antibody in PBS containing 1% NDS for one hour at room
747 temperature on a shaker protected from light. Cells underwent three 10-minute washes in PBS and
748 stained with DAPI for two minutes, followed by two quick washes with PBS. Coverslips were
749 mounted on glass slides (cat: 22-037-246, Fisher Scientific) using gelvatol mounting medium.

750

751 **Proximity Ligation Assay**

752 *Cells (Figures 1 and 3)*: Proximity ligation assay (PLA) was performed on an individual coverslip
753 in 24 well plates using Duolink In Situ PLA reagents (DUO92002, DUO920024, DUO92007
754 (orange) or DUO92014 (green), Sigma Aldrich). Cells were fixed, blocked/permeabilized, and
755 incubated in primary antibody solution as above and as previously described (*34*). Following
756 overnight primary antibody incubation (Table S4, for antibody details), cells underwent three 10-
757 minute washes in PBS. After washes, PLA was performed as described in (*34*). PLA incubation
758 steps took place in a humidified incubator at 37ºC with gentle agitation taking care that samples
759 did not dry out. For details of other products used see (*34*).

760

761 *Cells*: Proximity ligation assay (PLA) was performed in 16-well Nunc Lab Tek chamber slides
762 (cat: 178599, Thermo Fisher) using a NaveniFlex MR Kit (cat: NF.MR.100, Navinci). Cells were
763 fixed, blocked/permeabilized, and incubated in primary antibody solution as above and as
764 previously described (*34*). Following overnight primary antibody incubation (Table S4, for
765 antibody details), cells underwent three 10-minute washes in PBS. After washes, PLA was
766 performed according to manufacturer's protocol. PLA incubation steps took place in a humidified
767 incubator at 37ºC with gentle agitation taking care that samples did not dry out. For details of other
768 products used see (*34*).
769
770 *Rat brain tissue*: PLA was performed in blocked and permeabilized brain tissue as previously
771 described (*34*) using NaveniFlex Tissue MR Red (NT.MR.100.RED). Free floating tissue sections
772 were blocked and permeabilized in 1% triton-x (in PBS) containing 10% NDS for one hour at
773 room temperature on a shaker. Sections were then washed three times (10 minutes per wash) and
774 incubated in primary antibody solution (1% NDS in PBS) to label tyrosine hydroxylase (Table S4,
775 for antibody details) overnight at 4ºC on a shaker. The following day the tissue sections underwent
776 three 10-minute washes in PBS and were incubated in secondary antibody in PBS containing 1%
777 NDS for one hour at room temperature on a shaker protected from light. After secondary antibody
778 labeling, tissue sections were incubated overnight 4ºC on a shaker in primary antibody solution
779 containing the antibodies for PLA (Table S4, for antibody details). Next day, tissue sections
780 underwent three 10-minute washes in PBS and then were mounted on glass slides (cat: 22-037-
781 246, Fisher Scientific). See (*34*) for detailed description and video for mounting of tissue prior to
782 PLA. PLA was performed following the manufacturer's protocol. PLA incubation steps took place

783 at 37ºC ensuring that samples did not dry out. After PLA was completed, sections were covered
784 with a glass coverslip with gelvatol mounting medium.
785
786 **Animals**
787 All experiments utilizing animals were approved by the Institutional Animal Care and Use
788 Committee of the University of Pittsburgh. Male Lewis rats (8-9 months old) received a single
789 daily interperitoneal (i.p.) injection of 2.8 mg/kg of rotenone resuspended in 2% DMSO, 98%
790 miglyol 812 N as previously described (*45, 63*) until they reached behavioral endpoint (7-10
791 injections). Animals were euthanized using 0.3 mg/kg pentobarbital, followed by transcardial
792 perfusion. Brains were removed and postfixed in 4% paraformaldehyde for 24-h before placing
793 them 30% sucrose. Free-floating sections (35μm) were collected using a microtome and stored in
794 cyroprotectant at −20 °C until use.
795
796 **Cell lysis and western blot**
797 Cells were collected on ice in 1X Cell Signaling lysis buffer (cat:9803, Cell Signaling) containing
798 1:33 Halt Phosphatase Inhibitors (cat:78427, Thermo Fisher Scientific) and 1:100 Halt Protease
799 and Phosphatase Inhibitors (cat:78446, Thermo Fisher Scientific). Cells were lysed using a freeze-
800 thaw lysis method where cells were incubated in pulverized dry ice with ethanol for three minutes
801 followed by a warm water bath for three minutes and was repeated three times. Lysates were
802 clarified by centrifugation at 12,000 rpm for 10 minutes 4°C. Supernatant of the cell lysates were
803 collected, and protein quantified by Pierce BCA kit. 25-45μg of samples (dependent on target) was
804 mixed with 4X NuPAGE LDS Sample Buffer (supplemented with 5% β-mercaptoethanol and 10%
805 glycerol). Samples were run in duplicates on 4-12% NuPAGE or 10% NuPAGE Bis-Tris midi gels

806 with MOPS Running Buffer at 120 Volts for eight minutes followed by 200 Volts for 45 minutes.
807 At the end of electrophoresis, samples were transferred onto nitrocellulose membranes (0.2µm) at
808 100 Volts for 60 minutes on ice in prechilled transfer buffer (25mM Tris-Base, 198mM Glycine,
809 20% methanol v/v). Transferred membranes were blocked in Fish Serum Blocking Buffer
810 (cat:37527, Thermo Scientific) diluted in PBS (1:1 ratio) for one hour at room temperature on a
811 shaker. Membranes were incubated in primary antibodies (Table S4, for antibody details) diluted
812 in Fish Serum Blocking Buffer/PBS overnight at 4ºC on a shaker. The following day, membranes
813 were washed in PBS three times 10 minutes each and incubated in LiCor secondary antibodies
814 (Table S4, for antibody details). diluted in Fish Serum Blocking Buffer/PBS for 2 hours at room
815 temperature on a shaker. Membranes were washed three times in PBS for a duration of 10 minutes
816 each and imaged on an Odyssey LiCor CLx imaging system. Analysis was performed using Image
817 Studio software.
818
819 **Confocal microscopy and analysis**
820 Images were acquired on a Nikon Eclipse Ti2 Resonance Scan Spectral Confocal Microscope at
821 60X magnification using Nyquist criterion and resonant scanning. Laser parameters were set up
822 on positive and negative controls (e.g. primary antibody delete) to ensure there was no pixel
823 saturation. For quantitative comparisons all imaging parameters (e.g. laser power, gain, pinhole)
824 were held constant across an experiment. Confocal images were analyzed using Nikon NIS-
825 Elements Advanced Research software. For DHE fluorescence intensity analysis, regions of
826 interest were drawn around the signal on a per cell basis to obtain the fluorescence intensity. For
827 all other analyses, a binary layer was created using threshold parameters for each experiment and
828 used to identify each puncta or 'object'.

829 For Figures 1 and 3 images were acquired on Olympus BX61 confocal microscope at 60X
830 magnification (UPlansApo 60X) and Fluoview 1000 software (Melville, NY). Imaging parameters
831 were monitored to ensure that images were above background level and below pixel saturation.
832 For quantitative comparisons between groups, all imaging parameters (e.g. laser power, exposure,
833 and pinhole) were held constant across. For PL pS1292-LRRK2 (Figures 1 and 3, Sigma) intensity
834 analysis, regions of interest were drawn around the signal on a per cell basis to obtain the
835 fluorescence intensity. LRRK2$^{-/-}$ cells were used as assay controls.
836
837 *Colocalization Analysis:* Our protocol is similar to that of the University of Pittsburgh Center for
838 Biologic Imaging (*64*). Images are acquired on a Nikon A1R HD25 High-Definition Resonant
839 Scanning Confocal System with a 60X objective (1.4 NA) using Nyquist criterion. Exposure time
840 of each channel is kept consistent throughout sampling. Images were analyzed using NIS Elements
841 5.2 software. Separate binary layers are created for the 15-LO protein immunoreactivity and
842 PEBP1 signal. The intersection tool is then used to identify the third binary layer, the
843 "colocalization" mask, which corresponds to the overlapping immunoreactivity signals. The
844 threshold for each channel is kept consistent throughout the analysis per experiment. In this way,
845 the percent of 15-LO immunoreactivity (based on the binary mask) that colocalizes with PEBP1
846 signal is derived.
847
848 **Statistical Analysis**
849 Results are presented as mean ± SEM and are derived from 3 - 5 independent experiments. For
850 simple comparisons of two experimental conditions, two-tailed unpaired *t*-tests were used. Where
851 variances were unequal Welch's correction was used. For comparisons of multiple experimental

852 conditions, one-way or two-way ANOVA was used, and if significant overall, post hoc corrections
853 (with Tukey tests) for multiple comparisons were made. P-values less than 0.05 were considered
854 significant.
855
856 **References and Notes**
857

858 1. A. Zimprich *et al.*, Mutations in LRRK2 cause autosomal-dominant parkinsonism with
859 pleomorphic pathology. *Neuron* **44**, 601-607 (2004).

860 2. C. Paisan-Ruiz *et al.*, Cloning of the gene containing mutations that cause PARK8-linked
861 Parkinson's disease. *Neuron* **44**, 595-600 (2004).

862 3. J. Simon-Sanchez *et al.*, Genome-wide association study reveals genetic risk underlying
863 Parkinson's disease. *Nat Genet* **41**, 1308-1312 (2009).

864 4. J. H. Kluss, A. Mamais, M. R. Cookson, LRRK2 links genetic and sporadic Parkinson's
865 disease. *Biochem Soc Trans* **47**, 651-661 (2019).

866 5. E. Greggio *et al.*, Kinase activity is required for the toxic effects of mutant LRRK2/dardarin.
867 *Neurobiol Dis* **23**, 329-341 (2006).

868 6. A. F. Kalogeropulou *et al.*, Impact of 100 LRRK2 variants linked to Parkinson's disease on
869 kinase activity and microtubule binding. *Biochem J* **479**, 1759-1783 (2022).

870 7. L. Petropoulou-Vathi *et al.*, Distinct profiles of LRRK2 activation and Rab GTPase
871 phosphorylation in clinical samples from different PD cohorts. *NPJ Parkinsons Dis* **8**, 73
872 (2022).

873 8. E. M. Rocha, M. T. Keeney, R. Di Maio, B. R. De Miranda, J. T. Greenamyre, LRRK2 and
874 idiopathic Parkinson's disease. *Trends Neurosci* **45**, 224-236 (2022).

875 9. R. Di Maio *et al.*, LRRK2 activation in idiopathic Parkinson's disease. *Sci Transl Med* **10**,
876 (2018).

877 10. K. B. Fraser *et al.*, Ser(P)-1292 LRRK2 in urinary exosomes is elevated in idiopathic
878 Parkinson's disease. *Mov Disord* **31**, 1543-1550 (2016).

879 11. D. Jennings *et al.*, Preclinical and clinical evaluation of the LRRK2 inhibitor DNL201 for
880 Parkinson's disease. *Sci Transl Med* **14**, eabj2658 (2022).

881 12. S. H. Schmidt *et al.*, The dynamic switch mechanism that leads to activation of LRRK2 is
882 embedded in the DFGpsi motif in the kinase domain. *Proc Natl Acad Sci U S A* **116**, 14979-
883 14988 (2019).

884 13. S. H. Schmidt *et al.*, Conformation and dynamics of the kinase domain drive subcellular
885 location and activation of LRRK2. *Proc Natl Acad Sci U S A* **118**, (2021).

886 14. M. Steger *et al.*, Phosphoproteomics reveals that Parkinson's disease kinase LRRK2 regulates
887 a subset of Rab GTPases. *Elife* **5**, (2016).

888 15. J. H. Kluss *et al.*, Preclinical modeling of chronic inhibition of the Parkinson's disease
889 associated kinase LRRK2 reveals altered function of the endolysosomal system in vivo. *Mol*
890 *Neurodegener* **16**, 17 (2021).

891 16. W. M. Johnson, A. L. Wilson-Delfosse, S. G. Chen, J. J. Mieyal, The roles of redox enzymes
892 in Parkinson's disease: Focus on glutaredoxin. *Ther Targets Neurol Dis* **2**, (2015).

893 17. A. Mamais *et al.*, Arsenite stress down-regulates phosphorylation and 14-3-3 binding of
894 leucine-rich repeat kinase 2 (LRRK2), promoting self-association and cellular redistribution.
895 *J Biol Chem* **289**, 21386-21400 (2014).

896 18. X. Li, D. J. Moore, Y. Xiong, T. M. Dawson, V. L. Dawson, Reevaluation of phosphorylation
897 sites in the Parkinson disease-associated leucine-rich repeat kinase 2. *J Biol Chem* **285**, 29569-
898 29576 (2010).

899 19. S. Herbst *et al.*, LRRK2 activation controls the repair of damaged endomembranes in
900 macrophages. *EMBO J* **39**, e104494 (2020).

901 20. L. Bonet-Ponce *et al.*, LRRK2 mediates tubulation and vesicle sorting from lysosomes. *Sci*
902 *Adv* **6**, (2020).

903 21. T. Eguchi *et al.*, LRRK2 and its substrate Rab GTPases are sequentially targeted onto stressed
904 lysosomes and maintain their homeostasis. *Proc Natl Acad Sci U S A* **115**, E9115-E9124
905 (2018).

906 22. A. F. Kalogeropulou *et al.*, Endogenous Rab29 does not impact basal or stimulated LRRK2
907 pathway activity. *Biochem J* **477**, 4397-4423 (2020).

908 23. A. Bentley-DeSousa, S. M. Ferguson, A STING-CASM-GABARAP Pathway Activates
909 LRRK2 at Lysosomes. *bioRxiv*, 2023.2010.2031.564602 (2023).

910 24. X. Wang *et al.*, Membrane remodeling properties of the Parkinson's disease protein LRRK2.
911 *Proc Natl Acad Sci U S A* **120**, e2309698120 (2023).

912 25. S. J. Chapple, X. Cheng, G. E. Mann, Effects of 4-hydroxynonenal on vascular endothelial
913 and smooth muscle cell redox signaling and function in health and disease. *Redox Biol* **1**, 319-
914 331 (2013).

915 26. E. J. Jang *et al.*, Src Tyrosine Kinase Activation by 4-Hydroxynonenal Upregulates p38,
916 ERK/AP-1 Signaling and COX-2 Expression in YPEN-1 Cells. *PLoS One* **10**, e0129244
917 (2015).

27. R. Vatsyayan, H. Kothari, U. R. Pendurthi, L. V. Rao, 4-Hydroxy-2-nonenal enhances tissue factor activity in human monocytic cells via p38 mitogen-activated protein kinase activation-dependent phosphatidylserine exposure. *Arterioscler Thromb Vasc Biol* **33**, 1601-1611 (2013).

28. G. Leonarduzzi, F. Robbesyn, G. Poli, Signaling kinases modulated by 4-hydroxynonenal. *Free Radic Biol Med* **37**, 1694-1702 (2004).

29. G. Cohen *et al.*, Signaling properties of 4-hydroxyalkenals formed by lipid peroxidation in diabetes. *Free Radic Biol Med* **65**, 978-987 (2013).

30. Y. Riahi, G. Cohen, O. Shamni, S. Sasson, Signaling and cytotoxic functions of 4-hydroxyalkenals. *Am J Physiol Endocrinol Metab* **299**, E879-886 (2010).

31. D. Yang *et al.*, LRRK2 kinase activity mediates toxic interactions between genetic mutation and oxidative stress in a Drosophila model: suppression by curcumin. *Neurobiol Dis* **47**, 385-392 (2012).

32. J. Zhang *et al.*, Curcumin Reduced H2O2- and G2385R-LRRK2-Induced Neurodegeneration. *Front Aging Neurosci* **13**, 754956 (2021).

33. A. Hinman *et al.*, Vitamin E hydroquinone is an endogenous regulator of ferroptosis via redox control of 15-lipoxygenase. *PLoS One* **13**, e0201369 (2018).

34. M. T. Keeney, E. K. Hoffman, T. J. Greenamyre, R. Di Maio, Measurement of LRRK2 Kinase Activity by Proximity Ligation Assay. *Bio Protoc* **11**, e4140 (2021).

35. T. Kuwahara *et al.*, Roles of lysosomotropic agents on LRRK2 activation and Rab10 phosphorylation. *Neurobiol Dis* **145**, 105081 (2020).

36. J. T. Greenamyre, T. B. Sherer, R. Betarbet, A. V. Panov, Complex I and Parkinson's disease. *IUBMB Life* **52**, 135-141 (2001).

37. C. R. Trilling *et al.*, RedOx regulation of LRRK2 kinase activity by active site cysteines. *NPJ Parkinsons Dis* **10**, 75 (2024).

38. T. S. Fan *et al.*, Clinical heterogeneity of LRRK2 p.I2012T mutation. *Parkinsonism Relat Disord* **33**, 36-43 (2016).

39. A. U. Malik *et al.*, Deciphering the LRRK code: LRRK1 and LRRK2 phosphorylate distinct Rab proteins and are regulated by diverse mechanisms. *Biochem J* **478**, 553-578 (2021).

40. N. M. Ilieva, E. K. Hoffman, M. A. Ghalib, J. T. Greenamyre, B. R. De Miranda, LRRK2 kinase inhibition protects against Parkinson's disease-associated environmental toxicants. *Neurobiol Dis* **196**, 106522 (2024).

41. D. A. Quintero-Espinosa, S. Sanchez-Hernandez, C. Velez-Pardo, F. Martin, M. Jimenez-Del-Rio, LRRK2 Knockout Confers Resistance in HEK-293 Cells to Rotenone-Induced Oxidative Stress, Mitochondrial Damage, and Apoptosis. *Int J Mol Sci* **24**, (2023).

952 42. M. M. Gaschler, B. R. Stockwell, Lipid peroxidation in cell death. *Biochem Biophys Res*
953 *Commun* **482**, 419-425 (2017).

954 43. F. Martinez-Cruz, C. Osuna, J. M. Guerrero, Mitochondrial damage induced by fetal
955 hyperphenylalaninemia in the rat brain and liver: its prevention by melatonin, Vitamin E, and
956 Vitamin C. *Neurosci Lett* **392**, 1-4 (2006).

957 44. M. T. Keeney *et al.*, NADPH oxidase 2 activity in Parkinson's disease. *Neurobiol Dis* **170**,
958 105754 (2022).

959 45. E. M. Rocha *et al.*, LRRK2 inhibition prevents endolysosomal deficits seen in human
960 Parkinson's disease. *Neurobiol Dis* **134**, 104626 (2020).

961 46. A. Yoritaka *et al.*, Immunohistochemical detection of 4-hydroxynonenal protein adducts in
962 Parkinson disease. *Proc Natl Acad Sci U S A* **93**, 2696-2701 (1996).

963 47. A. Negre-Salvayre *et al.*, Pathological aspects of lipid peroxidation. *Free Radic Res* **44**, 1125-
964 1171 (2010).

965 48. S. E. Wenzel *et al.*, PEBP1 Wardens Ferroptosis by Enabling Lipoxygenase Generation of
966 Lipid Death Signals. *Cell* **171**, 628-641 e626 (2017).

967 49. K. Yeung *et al.*, Suppression of Raf-1 kinase activity and MAP kinase signalling by RKIP.
968 *Nature* **401**, 173-177 (1999).

969 50. L. F. Ye, B. R. Stockwell, Transforming Lipoxygenases: PE-Specific Enzymes in Disguise.
970 *Cell* **171**, 501-502 (2017).

971 51. C. X. Wu *et al.*, Parkinson's disease-associated mutations in the GTPase domain of LRRK2
972 impair its nucleotide-dependent conformational dynamics. *J Biol Chem* **294**, 5907-5913
973 (2019).

974 52. J. Lee, S. Giordano, J. Zhang, Autophagy, mitochondria and oxidative stress: cross-talk and
975 redox signalling. *Biochem J* **441**, 523-540 (2012).

976 53. M. Ghosh, F. Carlsson, A. Laskar, X. M. Yuan, W. Li, Lysosomal membrane permeabilization
977 causes oxidative stress and ferritin induction in macrophages. *FEBS Lett* **585**, 623-629 (2011).

978 54. C. Kubota *et al.*, Constitutive reactive oxygen species generation from
979 autophagosome/lysosome in neuronal oxidative toxicity. *J Biol Chem* **285**, 667-674 (2010).

980 55. S. Ray *et al.*, The Parkinson disease-linked LRRK2 protein mutation I2020T stabilizes an
981 active state conformation leading to increased kinase activity. *J Biol Chem* **289**, 13042-13053
982 (2014).

983 56. O. Carugo *et al.*, Vicinal disulfide turns. *Protein Eng* **16**, 637-639 (2003).

57. H. Zhu, F. Tonelli, D. R. Alessi, J. Sun, Structural basis of human LRRK2 membrane recruitment and activation. *bioRxiv*, 2022.2004.2026.489605 (2022).

58. H. S. Dhekne *et al.*, Genome-wide screen reveals Rab12 GTPase as a critical activator of Parkinson's disease-linked LRRK2 kinase. *Elife* **12**, (2023).

59. X. Wang *et al.*, Rab12 is a regulator of LRRK2 and its activation by damaged lysosomes. *Elife* **12**, (2023).

60. B. K. Chacko *et al.*, Pleiotropic effects of 4-hydroxynonenal on oxidative burst and phagocytosis in neutrophils. *Redox Biol* **9**, 57-66 (2016).

61. J. Wu *et al.*, STING-dependent induction of lipid peroxidation mediates intestinal ischemia-reperfusion injury. *Free Radic Biol Med* **163**, 135-140 (2021).

62. M. L. Selley, (E)-4-hydroxy-2-nonenal may be involved in the pathogenesis of Parkinson's disease. *Free Radic Biol Med* **25**, 169-174 (1998).

63. J. R. Cannon *et al.*, A highly reproducible rotenone model of Parkinson's disease. *Neurobiol Dis* **34**, 279-290 (2009).

64. N. Kumar *et al.*, Global and transcription-coupled repair of 8-oxoG is initiated by nucleotide excision repair proteins. *Nat Commun* **13**, 974 (2022).

Acknowledgments

Figure S15 was made using Biorender (Agreement #: FU26XHYZDS)

Funding:
National Institutes of Health grant R56 NS131137-01 (JTG)
The friends and family of Sean Logan (JTG)
The Blechman Foundation for Parkinson's Research (JTG)
The American Parkinson Disease Association Center for Advanced Research at the University of Pittsburgh (JTG)
The Michael J Fox Foundation Pritzker Prize (JTG)
Commonwealth of Pennsylvania Grant #601457

Author contributions:
Conceptualization: MTK, TGH, SAP, WDS, JTG
Methodology: MTK, SAP, WDS, TGH, JTG
Investigation: MTK, EKH, JW, WGW, SC, KF, MF, RDM, AK
Visualization: MTK, SAP, WDS, JTG
Funding acquisition: JTG
Project administration: MTK, JTG
Supervision: JTG
Writing – original draft: MTK, JTG
Writing – review & editing: MTK, EMR, TGH, SAP, WDS, JTG

Competing interests: WDS and SAP are full-time employees of Acurex Biosciences and also own stock in the company. AK is a paid consultant of Acurex Biosciences.

Data and materials availability: All data are available in the main text or the supplementary materials.